JOURNAL OF MAGNETIC RESONANCE **134,** 88–112 (1998)
ARTICLE NO. MN981470

Off-Resonance Proton Decoupling On-Resonance and Near-Resonance

A Close Look at ^{13}C CPMAS Linewidths in Solids for Rigid, Strongly Coupled Carbons under CW Proton Decoupling

D. L. VanderHart*,[1] and G. C. Campbell†

*Polymers Division, National Institute of Standards and Technology, Gaithersburg, Maryland 20899; and
†Central Research, Du Pont Company, Wilmington, Delaware 19880

Received June 26, 1997; revised April 1, 1998

Ambient-temperature ^{13}C linewidth (LW) and transverse relaxation (T_2^C) data are presented for the natural-abundance crystalline carbons of linear polyethylene (LPE) under CW proton decoupling conditions and magic angle spinning (MAS). This linewidth behavior typifies that seen for rigid methylene carbons whose attached protons are also strongly coupled to other protons. These data are presented for two LPE samples (unoriented, melt-crystallized and uniaxially oriented, extruded) as a function of several parameters including static field (1.4 T < B_0 < 9.4 T), proton decoupling field strength (38 kHz < ν_1^H < 90 kHz), MAS frequency (0.5 kHz < ν_r < 8 kHz) and RF frequency offsets from resonance (−4 kHz < $\Delta\nu_{off}$ < 4 kHz). It is the ubiquitous nature of off-resonance proton irradiation (ORPI) (arising from fixed or rotationally dependent deviations from the true proton resonance condition) which provides the focus for this work. Corresponding contributions, LW(ORPI), to the total LW are treated within the general framework of the effective-field picture of CW decoupling. Then, considering the presence of spin fluctuations characteristic of the strongly-dipolar-coupled protons of LPE, LW(ORPI) can be traced to orbit-dependent T_2^C contributions to LW. Important dependences demonstrated and discussed include: (1) For "off-resonance" decoupling, there is a quadratic dependence of LW(ORPI) on ($\Delta\nu_{off}/\nu_1^H$) *and* there is a strong dependence of the corresponding parabolic coefficient on ν_r. From the latter dependence, characteristic times for spin fluctuations are also estimated. (2) For "on-resonance" decoupling, LW(ORPI) is proportional to $(\nu_1^H)^{-2}$ *and* shows very little sensitivity to ν_r. These LW(ORPI) contributions become more important at higher B_0 since the principle reason for ORPI is the chemical shift anisotropy (CSA) of the ^{13}C-bonded protons. The difference in sensitivities of LW(ORPI) to ν_r for the off-resonance and the on-resonance cases is traced back, respectively, to the scalar property of $\Delta\nu_{off}$ for RF frequency offsets and to the tensorial character of the proton CSA. Contributions from LW(ORPI), possibly much larger than those seen in LPE, can be expected when protons near ^{13}C nuclei sense any non-scalar, rotor-position-dependent magnetic fields, e.g., (a) local dipolar fields associated with third, magnetic nuclei or (b) perturbing magnetic-susceptibility fields arising from paramagnetic or ferromagnetic inclusions in a sample. By understanding the contributions to LW in LPE, one can forecast much more precisely what the potential benefits will be from new decoupling schemes like the recently reported "two-pulse phase modulation" (TPPM) since TPPM is designed to reduce LW(ORPI). Aside from LW(ORPI) contributions, the experimental LW data cover parameter space where another broadening mechanism, namely, MAS-assisted dipolar fluctuations (MADF), is seen. This mechanism, also recognized by others, creates a T_2^C-type linewidth contribution which increases rapidly as ν_1^H decreases and which additionally has some orbit dependence. If the current trend in ^{13}C CPMAS is toward higher B_0 and ν_r, the ν_r-dependent MADF contributions can easily dominate LW relative to the B_0-dependent LW(ORPI) contributions. One can avoid serious MADF broadening; however, the minimum acceptable values of ν_1^H for good decoupling rise rapidly with B_0. Finally, a few LW measurements are made on methyl-α-D-glucopyranoside tetraacetate (MGT), a rigid, polycrystalline material containing carbons with 0, 1, 2, and 3 attached protons. The behaviors of the methylene, methine, and methyl carbons at 9.4 T are compared with the behavior of LPE.

Key Words: **resolution; ^{13}C; CPMAS; decoupling; methylene; polyethylene.**

I. INTRODUCTION

Good resolution in CPMAS spectra is very desirable. With the trend toward performing CPMAS experiments at higher static fields, one may encounter mechanisms for degrading resolution which were not so important at lower fields. The challenge for finding ways to circumvent these mechanisms is ever present. Recently (*1*), a phase modulation scheme, called two-pulse phase modulation (TPPM) was shown to give significant improvement in resolution at 9.4 T for strongly coupled systems. Even more recently (*2*), Ernst *et al.* demonstrated experimentally and calculated theoretically the behavior of the

[1] To whom correspondence should be addressed.

1090-7807/98 $25.00

^{15}N spectrum in an isolated, strongly coupled two-spin (^{15}N–^{1}H) system. In the latter case, proton spin-exchange with other protons is slow so that second-order couplings between the heteronuclear dipolar interaction and the proton chemical shift anisotropy create significant splitting and broadening of the ^{15}N resonance. The motivation for the latter study was to understand and exploit this second-order effect and show how, using TPPM, one may eliminate these second-order effects.

Contributions to solid-state linewidths in ^{13}C CPMAS spectra have varied origins (*3–5*), and the presence or absence of molecular motion is often important for determining linewidths (*3–7*). In this paper, we are more concerned with those mechanisms contributing to linewidth for the rigid lattice where motional contributions are negligible. One such mechanism which has been recognized (*1, 2, 4, 5, 8–12*) as contributing to linewidth is off-resonance proton irradiation (ORPI) and some efforts (*10–12*) have focused specifically on materials which have resonance offsets traced to large magnetic-susceptibility perturbations. It is now well recognized that good decoupling of the heteronuclear (we will assume ^{13}C–^{1}H nuclei in this paper) dipolar interaction requires that one be "on-resonance" for the proton. Each proton, however, at any point in time, might be slightly "off-resonance" because of (a) varied isotropic shifts for different protons, (b) chemical shift anisotropy (CSA) for each proton, (c) field variations (large in paramagnetic materials or materials with ferromagnetic inclusions) arising from both isotropic and anisotropic bulk magnetic susceptibility effects, (d) inhomogeneities in the applied field, and/or (e) dipolar fields originating from a third nuclear species. Given that at least the first three of the five foregoing effects scale with the static field, one will have to pay more careful attention to this mechanism at higher fields.

In this paper, we present extensive data on resolution in crystalline polyethylene (PE), which is an example of a natural-abundance carbon population in a strongly coupled system. All carbons are chemically identical methylene carbons whose dominant dipolar interaction is heteronuclear and stems from their attached protons. Each of the protons, on the other hand, while strongly coupled to its geminal partner at 0.178 nm, has 4 other nearest neighbors at a distance of about 0.25 nm and 11 more within 0.31 nm. Thus, the network of coupled spins is large. All of our data are taken with CW irradiation of the protons. A substantial portion of these data was presented at the Experimental NMR conference in 1990 and we have not published our results previously because we did not understand certain phenomena associated with on-resonance decoupling; we think we understand them better now. Data were taken over a range of static fields from 1.4 to 9.4 T, over RF fields from 38 to 90 kHz, over spinning speeds from 0.5 to 8 kHz, and over RF frequency offsets up to 4 kHz. We felt that these data would be a useful contribution to the general discourse on resolution, since there are some features which should be appreciated, at least qualitatively. Also of interest is the fact that this study reveals something about the nature of spin fluctuations in a strongly coupled spin system.

We adopt a very simplified physical picture for off-resonance decoupling, knowing that the mathematical framework for the more exact theory has been presented before (*8*). The simple view is that one is trying to use RF irradiation to make the expectation values $\langle I_{zi}\rangle$ of the proton spins as close to zero as possible during proton irradiation (z is defined as parallel to the static field). A ^{13}C nucleus, which we assume to be isolated from other ^{13}C nuclei, senses protons at distances r_i because it is coupled to the protons through the *residual* dipolar interaction, $H_{\mathrm{Dr}}^{\mathrm{IS}}$ (in rad/s), given by

$$H_{\mathrm{Dr}}^{\mathrm{IS}} = (\mu_0/4\pi) \sum_i \gamma_{\mathrm{C}}\gamma_{\mathrm{H}}\hbar\,(r_i)^{-3}(1 - 3\cos^2\theta_i)S_z\langle I_{zi}\rangle$$

$$= \sum_i \omega_{\mathrm{D}i} S_z \langle I_{zi}\rangle, \qquad [1]$$

where, for a dilute, natural-abundance methylene carbon considered here, with spin S_z, the dominant interactions will stem from the two attached protons. Other constants in Eq. [1] have their usual meanings and are given in SI units. Equation [1] expresses the idea that for the heteronuclear interaction the dominant interaction takes place between the z-components of the respective spins. (We will, for the time being, ignore the second-order shift and broadening (*13, 14*) arising from nonsecular terms of the heteronuclear dipolar coupling; these effects become very small at high fields.) From Eq. [1] we can adopt four immediate perspectives. First, all perturbations on the ^{13}C resonance arising from Eq. [1] are, in a real sense, "filtered" through $\omega_{\mathrm{D}i}$, which includes angular dependence. While the focus of the effort to achieve better resolution via better decoupling strategies is to manipulate only the proton spins (the $\langle I_{zi}\rangle$ term), the carbon is influenced by this term in a more complicated way, namely, via the residual proton local field, $\omega_{\mathrm{D}i}\langle I_{zi}\rangle$. Second, the sources of broadening (*4, 5*) associated with the ^{13}C environment in the absence of the proton dipole moments will be unaffected by manipulating the proton spins; such broadening includes magnetic field inhomogeneity, anisotropic bulk magnetic susceptibility (ABMS) effects, conformationally induced chemical shift dispersions (*15, 16*), shifts arising from inequivalences in crystal packing (*17*), etc. This second point is intuitively obvious; nevertheless, some improvement in resolution through the manipulation of proton spins is observed, e.g., in paramagnetic materials with large susceptibilities (*10–12*). Large susceptibility shifts have a direct effect on both the proton and the ^{13}C resonances. In addition to this direct shift, the ^{13}C resonances are broadened because off-resonance proton irradiation causes $\langle I_{zi}\rangle$ values to become appreciable, thereby making contributions from Eq. [1] large. The latter type of broadening is one that can be altered with different proton irradiation strategies. Given that the separation of the "Pake doublet" (*18*) for an isolated,

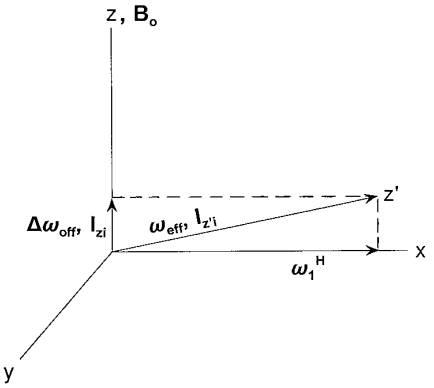

FIG. 1. Effective-field picture for a proton spin, I_i, in the presence of an RF field of amplitude, ω_1^H, and resonance offset, $\Delta\omega_{off}$. The effective field, ω_{eff}, defines the direction, z', along which the proton spin is quantized ($I_{z'i}$). However, any ^{13}C nucleus near this proton interacts most strongly with the "static" projection of I_i, I_{zi}, which lies along B_0.

unirradiated ^{13}C–^1H spin pair separated by 0.11 nm is about 22 kHz, a perspective on effective decoupling is that one would like $|\langle I_{zi}\rangle|$ to be no more than about 10^{-3} to 10^{-4} times its unperturbed value of 0.5. Thus, effective decoupling requires a very high degree of averaging.

A third perspective about Eq. [1] is that magic angle spinning (MAS) will, in general, cause the proton resonance offset, $\Delta\omega_{off}$, arising from the five sources previously mentioned, to be modulated. In the limit of a proton RF field, large compared with the ^{13}C–^1H and ^1H–^1H dipolar interactions and large compared with the other resonance offsets as well,

$$|\langle I_{zi}\rangle| \approx 0.5(\Delta\omega_{off}/\omega_{1H}), \qquad [2]$$

where ω_{1H} is the on-resonance angular proton nutation frequency associated with the proton RF field. Figure 1 illustrates this concept using the familiar "effective-field" picture (*19*) of proton irradiation in the rotating frame of the proton RF. When ω_{1H} is much larger than ω_{Di}, ω_{off}, and ω_{Dij}, the dipolar coupling between protons, then the protons are, to a good approximation, quantized along ω_{eff}, the "effective field," which is the vector sum of $\Delta\omega_{off}$ and ω_{1H}. The projection, I_{zi}, of such a quantized proton spin in the direction of the static field is approximately $(\Delta\omega_{off}/\omega_{1H})I_{z'i}$, where z' lies along ω_{eff}. If, in this picture, the lifetime of the $I_{z'i}$ states is very long, then the ^{13}C resonance, at any point in the rotor cycle, would be shifted by the amount $\Delta\omega_s$, where

$$\Delta\omega_s = \sum_i (\omega_{Di}\Delta\omega_{off}/\omega_{1H})I_{z'i}. \qquad [3]$$

With all values of $I_{z'i}$ in the high temperature approximation taken into account, $\Delta\omega_s$ gives rise to a resonance pattern symmetric about that instantaneous ^{13}C resonance position, ω_C, which would pertain in the absence of the proton–carbon dipolar interaction. For example, a simple splitting (or a miniature Pake pattern (*18*)) would be associated with an isolated ^{13}C–^1H pair in a static single crystal (or in a static powder sample). With MAS, ω_C, ω_{Di}, and $\Delta\omega_{off}$, in general all become time dependent and if the MAS average of ω_C has no appreciable dispersion, when averaged over all such carbons in the sample, then the resulting lineshape will be governed by the MAS average of $\Delta\omega_s$. As has been amply documented (*2*), since ω_{Di} is a second-rank tensor, the product in the numerator of Eq. [2] will, in general, correspond to a sum of tensors of different ranks. For example, if $\Delta\omega_{off}$ is also second rank (e.g., suppose $\Delta\omega_{off}$ is the proton CSA tensor), then the product consists of the sum of tensors of ranks 0, 2, and 4. MAS only averages to zero the part of the product which has rank 2. The part having rank 0 is unaveraged by MAS and gives rise to a fixed splitting, i.e., shifts whose sign depends on the sign of $I_{z'i}$; the part having rank 4 is partially averaged and leads to an inhomogeneous line broadening. On the other hand, if $\Delta\omega_{off}$ is simply an offset of the proton transmitter, then $\Delta\omega_s$ is a pure second-rank tensor and MAS averages it to zero. Isotropic bulk susceptibility effects give rise to a $\Delta\omega_{off}$ which is a second-rank tensor; anisotropic bulk magnetic susceptibility produces a $\Delta\omega_{off}$ which includes tensorial character of orders 0, 2, and 4 with the result that $\Delta\omega_s$ will be even more complex. Finally, magnetic field inhomogeneity is not confined to a tensor of a particular order. Thus, the influence of MAS is not simple, and, in general, MAS provides only incomplete averaging when the lifetime of the $I_{z'i}$ spin state is long compared to a rotor period. Implementation of double rotation (*20*) (DOR) or dynamic angle spinning (DAS) techniques (*20–22*) which simultaneously average over second- and fourth-order tensors have been shown (*2*) to be effective in this context. Table 1 summarizes the tensorial rank, typical range, and B_0 dependence of various sources of resonance offset.

The above scenario including the influence of MAS averaging is predicated on there being long-lived proton spin states. But, in strongly coupled systems, irradiated on-resonance, fluctuations of the proton spins along their quantization axes, i.e., along ω_{eff}, occur rather briskly, i.e., about half as fast as the fluctuations along the static-field direction in the laboratory frame (the secular proton–proton dipolar Hamiltonian in the rotating frame is halved relative to the Hamiltonian in the laboratory frame (*8*)). Indeed, in the usual application of CPMAS NMR, it is recognized that resolution is greatly aided (*23*) by these fluctuations. The time dependence of the proton spin is not random (*24*), but is a complex behavior of a many-body spin system undergoing mutual spin exchange *while conserving overall rotating-frame Zeeman polarization.* If one looks at a particular spin, however, one might expect the fluctuations to have considerable random qualities. If, in Eq. [1], the time average of $\langle I_{zi}\rangle$ were identically 0, then this fluctuation, *if rapid enough*, would average to 0 (or "decouple") the perturbing interaction given by Eq. [2]. In the limit where this fluctuation time is rapid, relative to the rms

TABLE 1
Different Sources for Instantaneous Departures from Proton Resonance during MAS

Source	Tensor rank	Typical range	B_0 dep.
1. σ^{H} dispersion	0	1 ppm	1
2. $\Delta\sigma^{H}$	2	5 ppm	1
3. χ^{a}	2	1.5 ppm	1
4. $\Delta\chi^{b}$	0, 2, 4	1 ppm	1
5. B_0 inhomogeneity	?	0.1 ppm	?
6. Het. dipolar: ω_{X-H}	2	? (kHz)[c]	0

Note. Included are the tensorial rank *of the associated perturbing magnetic fields at a proton nucleus,* estimates of their typical ranges, and the dependence of these fields on B_0.

[a] Perturbing fields arising from distant spherical volumes having isotropic bulk magnetic susceptibility. Net instantaneous resonance displacements are traced to non-ellipsoidal particle shape and the shape and distribution of neighboring particles. The given range assumes that all particles are diamagnetic. If particles are paramagnetic or ferromagnetic, then the instantaneous departures from resonance can become much larger than 1.5 ppm.

[b] Perturbing fields arising from distant volumes having anisotropic bulk magnetic susceptibility.

[c] The local dipolar fields from "third" magnetic nuclei cover a range from 0 to 35 kHz, the latter for protons geminal to ^{19}F nuclei.

couplings given by Eq. [3], then one would be in a "weak coupling" regime where the fluctuations would create an uncertainty broadening in the linewidth, thereby giving rise to a T_2^C(ORPI) of the general form

$$\mathrm{LW(ORPI)} = [\pi T_2^{C}(\mathrm{ORPI})]^{-1} \propto \sum_i (\omega_{Di}\langle I_{zi}\rangle)^2 J_i(0), \quad [4]$$

where $J_i(0)$ is the spectral density of fluctuations at zero frequency for proton i and LW(ORPI) is the corresponding homogeneous contribution to the observed linewidth arising from off-resonance effects.

The issue of whether the time average of $\langle I_{zi}\rangle$ is zero is interesting to consider before we look at the data. Over long times, the high temperature approximation forces $\langle I_{zi}\rangle$ to average to zero to a degree beyond our ability to detect it. However, in the case we have before us, there are characteristic times, such as the rotor period, T_r, over which it is important to understand the completeness of the averaging of $\langle I_{zi}\rangle$. Each carbon has a statistically distributed local Zeeman polarization associated with n of its closest neighbors. *Since spin exchange is conserving of total polarization,* one might well suppose that, averaged over any given time, $\langle I_{zi}\rangle$ for a proton bound to a ^{13}C nucleus would approximately reflect the average I_z value of the proton spins over some corresponding radius. One would further anticipate, based on statistical arguments alone, that the longer the time of averaging, the larger the number of spins whose conserved total spin contributed to that average; hence, the closer to zero $\langle I_{zi}\rangle$ would become. The "diffusive" nature of polarization transport in dipolar-coupled spin systems, such as that of the protons, may imply that the rate of this final decay toward zero of the statistical fluctuations is relatively slow.

As one can see from Eqs. [2] and [3], one can consider resolution to be degraded from ORPI effects through inhomogeneous broadening (Eq. [2]) or homogeneous broadening (Eq. [3]). Obviously, in a case like LPE, one cannot expect the inhomogeneous view to be correct since we know the spins are strongly coupled and we know that strong dipolar fluctuations are present (*4*, *25*). In fact, for a static oriented (OR) LPE sample with unique axis along B_0, the characteristic spin fluctuation time, τ_{sL}, pertaining to the *laboratory frame,* is deduced (*25*) to be 24 μs. Moreover, spin geometry at that particular orientation is such that proton spin flips within the $^{13}CH_2$ group do not contribute to τ_{sL}. (Other estimates (*4*), τ_{sL} = 16 to 18 μs, have also been offered for LPE and OR-LPE samples in the presence of MAS, but, as will be seen, the analysis used to obtain τ_{sL} was not entirely appropriate.) For the problem addressed here, we must consider the characteristic fluctuation time, τ_s, in the *rotating* frame. For larger values of ν_1^H, we expect that $\tau_s = 2\tau_{sL}$.

To the degree that fluctuations do not completely average $\langle I_{zi}\rangle$ to zero over a rotor period, i.e., over a few times τ_s, one might take the view that some portion of the ORPI-related influence on linewidth is subject to coherent averaging via MAS itself or possibly TPPM (*1*). Then it becomes a question of particular interest to understand the origin of ^{13}C linewidths under "on-resonance" CW decoupling and how spinning speed or the frequency of TPPM modulation influences these linewidths. Unfortunately, we do not have access to the hardware whereby flexible (*1*) TPPM sequences can be implemented. So the application of schemes like TPPM will be left to others.

EXPERIMENTAL

NMR Spectrometers, Pulse Sequences, and RF Field Calibrations

Data at 1.4 T included herein have been published and described previously (*4*). We no longer have access to this electromagnet-based spectrometer. The 2.35 T spectrometer and probe are non-commercial although the probe incorporates a 7-mm rotor/stator made by Doty Scientific, Inc. (*26*). The 4.7 T spectrometer is a Bruker CXP-200 with probe made by Doty Scientific, Inc. The 9.4 T spectrometer and probe were made by Chemagnetics; the associated high-power amplifiers were not manufactured by Chemagnetics. For the longest decoupling pulses used, RF droop in amplitude on the 2.35 T spectrometer is too small to measure (<1%); droop on the 4.7 T spectrometer is about 3%, with changes occurring over the entire decoupling period. Droop on the 9.4 T instrument is <1% after a slight change during the first 100 μs. There is also longer-time drifting of RF amplitudes over a few percentage points in

this 9.4 T instrument; amplitude stability is about 1% at 4.7 T and very good at 2.35 T.

We also conducted some experiments at 8.5 T using another Chemagnetics system. Results are consistent with, but not as extensive as, the 9.4 T data; hence, we do not report the 8.5 T results except to note that we measured temperature-dependent linewidths, on-resonance, for LPE using an RF amplitude, ν_1^H, of about 84 kHz and a rotor frequency, ν_r, of 4 kHz. Observed linewidths were 29.2 $\pm$ 0.5 Hz at both -50°C and 23°C. At 70°C the linewidth increased to 32.0 $\pm$ 0.5 Hz. The main inference from these data is that the *contributions to ambient-temperature linewidths from molecular motion are likely to be very small for the crystalline carbons of LPE.* Other observations reported herein corroborate this.

Pulse sequences used were very straightforward; each involved the same initial preparation (*27*) of the ^{13}C magnetization associated with the LPE crystalline regions. This preparation included a 1 ms CP time, a storage of this ^{13}C magnetization alternately parallel and antiparallel to B_0, a 3 s delay (during which the ^{13}C signal from the LPE crystalline region is selected since the non-crystalline carbons of LPE fully relax), and a final 90° ^{13}C pulse immediately preceding observation. At 2.35 and 9.4 T, any amplitude and frequency changes necessary for decoupling occurred immediately following this 90° observation pulse; at 1.4 and 4.7 T, proton RF characteristics for CP and decoupling were identical. Measurement of T_2^C follows the same recipe for the preparation of the magnetization; however, observation is delayed by a variable decoupling interval of length equal to an even number of rotor periods; also, a 180° ^{13}C pulse is centered in this interval to refocus ^{13}C chemical shift effects. (At 2.35 and 9.4 T, the amplitude and/or frequency of the proton RF was altered only during this interval.) T_2^C is determined from the change of intensity with echo time, i.e., with interval length. The first point in these plots is always the amplitude after two rotor periods; hence, especially at lower ν_r, any rapid initial decay is not taken into account.

Measurements of the proton RF amplitudes, ν_1^H, were made by calibrating one RF field, usually near 70 kHz, by means of determining the lengths of 180° and 360° proton pulses. The expected null signals accompanying such pulses were detected indirectly via the ^{13}C signal, obtained by CP, following these proton pulses. Other values of the proton RF field were measured by monitoring the ratios of secondary amplitude measurements, referenced to the corresponding measurement at the calibrated field. These secondary measurements were made with an oscilloscope in several ways, namely, via a weakly coupled, fixed antenna (2.35 T), monitoring through the ^{13}C probe port (4.7 T), and forward-power measurements using an in-line directional coupler (9.4 T). Adjustments were made at 9.4 T to account for the initial small-but-rapid change in RF level during a pulse. Absolute errors (95% confidence level) in the measurement of RF levels obtained in this way (neglecting drifts in amplitude), are estimated to be $\pm$2%; relative errors associated with the oscilloscope readings are an additional $\pm$1%.

Materials

Unoriented linear polyethylene (LPE) samples were machined from melt crystallized plugs of NIST's standard reference material, SRM 1475 LPE (M_n = 18,300 and M_w = 52,000). The oriented LPE (OR-LPE) was obtained from Ian Ward and was extruded through a conical die at 90°C with a draw ratio of 16. This material has uniaxial orientation; the draw direction is placed parallel to the rotor axis. The OR-LPE starting material is a linear PE with M_n = 25,500 and M_w = 135,000. Samples were machined to the appropriate ID of the rotors, 6.0 mm for the 2.35 and 4.7 T rotors and 4.5 mm for the 9.4 T rotor. Sample lengths were limited to approximately 0.6 times the RF coil length. The methyl-α-D-glucopyranoside tetraacetate (MGT) was a commercial, polycrystalline sample obtained from Dr. B. Coxon at NIST; this material was used as received.

RESULTS

In this section we mainly present the phenomenology. Interpretation will be the focus of the Discussion. We will use the abbreviation LW to refer to linewidths (full width at half height). Since we will separately present data using on-resonant and off-resonant proton irradiation, we will distinguish the LW associated with "on-resonance" or "off-resonance" proton irradiation by the subscripts "n" or "f," respectively; e.g., the observed linewidths are LW_n(obs) and LW_f(obs). We will also freely substitute symbols using ν (in Hz) corresponding to previously defined ω terms (in rad), e.g., $2\pi\nu_1^H = \omega_1^H$. Nearly as many measurements were conducted on the OR-LPE samples as were performed on the LPE samples. For clarity, however, a much smaller portion of the OR-LPE data will appear in the figures, relative to the LPE data.

Spectra

Figure 2 shows a typical spectrum for crystalline LPE (8 scans), taken at 2.35 T with ν_1^H = 71 kHz. The absence of any downfield intensity verifies the effectiveness of the 3 s delay time in Torchia's (*27*) T_1^C method, thereby eliminating signals originating from the non-crystalline region as well as minimizing signals from certain interfacial regions (*28*). This lineshape is not Lorentzian; a Lorentzian fit yields a line whose peak is about 10% higher and whose wings are slightly more intense. The linewidth shown in Fig. 2 is 7.40 Hz while a Lorenztian fit gives 6.55 Hz. The linewidths reported here are actually measured at half height; they are not the widths from Lorentzian fits. Qualitatively, deviations from Lorentzian shapes ranged from zero to "modest," where the largest deviations were seen using off-resonant irradiation; the deviations were greater for

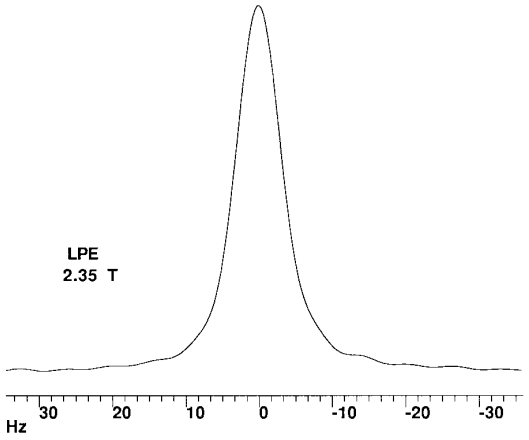

FIG. 2. Eight-scan lineshape for the crystalline carbons of linear polyethylene at 2.35 T. On-resonance decoupling is used; $\nu_1^H = 71$ kHz and $\nu_r = 2.0$ kHz. Full width is 7.40 Hz; best Lorentzian fit gives 6.55 Hz. The lineshape is quite symmetric under these conditions.

irradiation on one side of resonance, usually the downfield side at higher B_0.

Off-Resonance Linewidth Behavior

Much is recognized (*4, 5, 8, 9*) regarding the influence on the carbon linewidth when protons are irradiated off-resonance. We define $\Delta\nu_{RF}$ to be the deviation (in Hz) from the ν^*_{RF} where LW(obs) is a minimum; we presume that ν^*_{RF} is at or near the true isotropic-average proton resonance. Experimentally it is found (*4, 9*), and theoretically it is predicted (*8*), that in the presence of proton spins whose projections along ω_{eff} fluctuate as a result of spin exchange, there should be a quadratic dependence of linewidth on $\Delta\nu_{RF}$ according to the equation

$$LW_f(\text{obs}) = a + b(\Delta\nu_{RF})^2 = a + LW_f(\text{ORPI}), \qquad [5]$$

where $a = LW_n(\text{obs})$, b is the parabolic coefficient, and $LW_f(\text{ORPI})$ is identified with the quadratic term. In addition, the effective field picture of Fig. 1 predicts that this coefficient, b, should have a dependence on $(\nu_1^H)^{-2}$ in the limit of large RF fields (see Eqs. [2] and [4]).

Figure 3 shows the expected quadratic dependence of linewidth on $\Delta\nu_{RF}$ for five cases at 2.35 T. It is on the basis of a fit to a full curve (both positive and negative values of ν_{RF}) that ν^*_{RF} is established. Not shown is the observation that full curves for LPE and OR-LPE do not give the same ν^*_{RF} values. Whereas the ^{13}C resonance positions remain fixed, the ν^*_{RF} value for OR-LPE is about 0.6 ppm higher than that for LPE. We will discuss the origin of this apparent shift later. Three other points are qualitatively illustrated. First, at a fixed ν_r, the coefficient, b, decreases when ν_1^H increases, as just discussed. Second, b decreases as ν_r increases at fixed ν_1^H, a point which may not be widely recognized. Third, for the same ν_r and ν_1^H, the oriented sample (OR-LPE) has a smaller b than the melt-crystallized, unoriented material. Note that we will use the designation "LPE" to refer exclusively to this unoriented, melt-crystallized sample. Also, by virtue of being uniaxially oriented with its unique axis parallel to the rotor axis, the OR-LPE should behave like a single crystal in that for all crystalline carbons, only one orbit of orientations is explored during each rotor cycle. Therefore, in the sense that the OR-LPE sample represents a single orientation within the LPE sample, Fig. 3 demonstrates the existence of an *orientation-dependent dispersion* of LWs within the LPE sample.

Figures 4–6 focus on the parabolic coefficient, b, in Eq. [5]. Figure 4 shows the dependence, at 2.35 T, of b on ν_r at several values of ν_1^H. Also shown is a test for the uniformity of that dependence of b on ν_r. Each curve is multiplied by a constant such that the initial value is 12. From the lack of any systematic trend in the distribution of points at any given value of ν_r for these "scaled" curves, we conclude that within experimental error, *the fractional change in b upon changing* ν_r *is independent of* ν_1^H *from* 44 *to* 71 *kHz.*

Figure 5 tests the hypothesis that, at a given ν_r, b is proportional to $(\nu_1^H)^{-2}$. It is shown that the dependence of b on $(\nu_1^H)^{-2}$ is quite linear for ν_1^H from 44 to 71 kHz; however, for reasons that we do not understand, an extrapolation of the slopes in Fig. 5 suggests that b would become zero, independent of ν_r, at a finite value of ν_1^H, namely ≈140 kHz, rather than at infinite RF power. Nevertheless, Fig. 5 indicates that b is approximately proportional to $(\nu_1^H)^{-2}$.

Figure 6 demonstrates two points. First, b has no significant dependence on B_0, in keeping with the idea that when $\Delta\omega_{RF}$ dominates $\Delta\omega_{off}$ (see Eqs. [2] and [4]), there is no

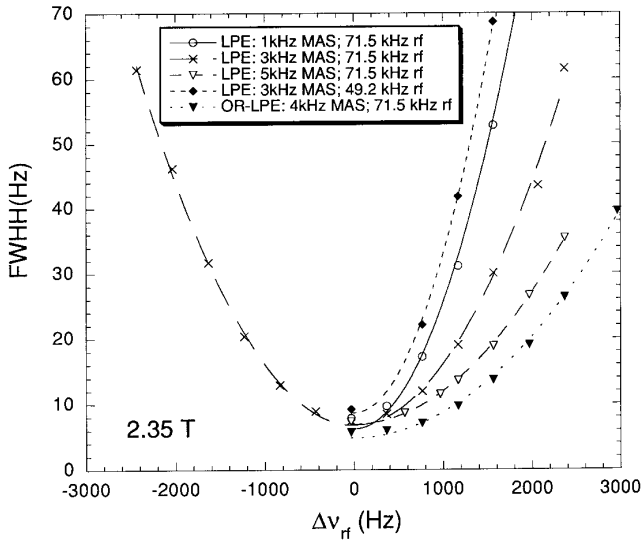

FIG. 3. Observed linewidths at 2.35 T as a function of relative decoupler frequency for the samples and conditions given in the legend. Parabolic shape defined in Eq. [5] is generally found, but the parabolic coefficient, b, depends on ν_r and ν_1^H. In addition, contrast in the OR-LPE and LPE behavior indicates that b is orbit-dependent. Lines through the points are parabolic fits.

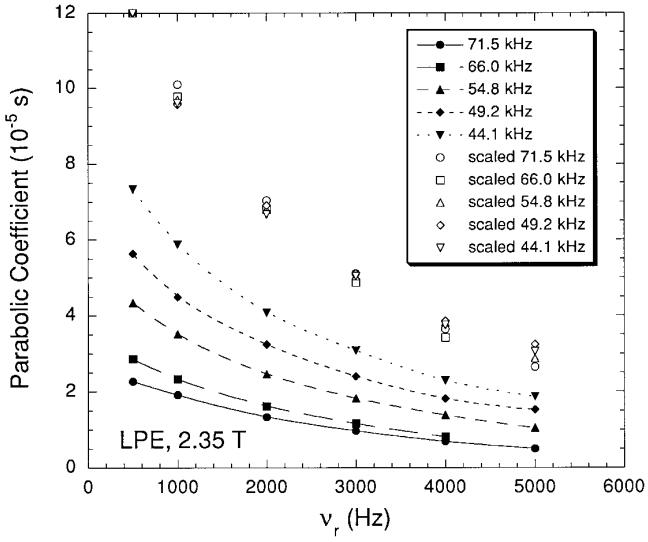

FIG. 4. Dependence of the parabolic coefficient on spinning frequency at 2.35 T for LPE at the various RF field strengths indicated in the legend. A rescaling of these coefficients such that for $\nu_r = 500$ Hz, all coefficients are the same, shows that the fractional change in this coefficient with ν_r is not sensitive to ν_1^H. Lines through the points are interpolated and for visual clarity only.

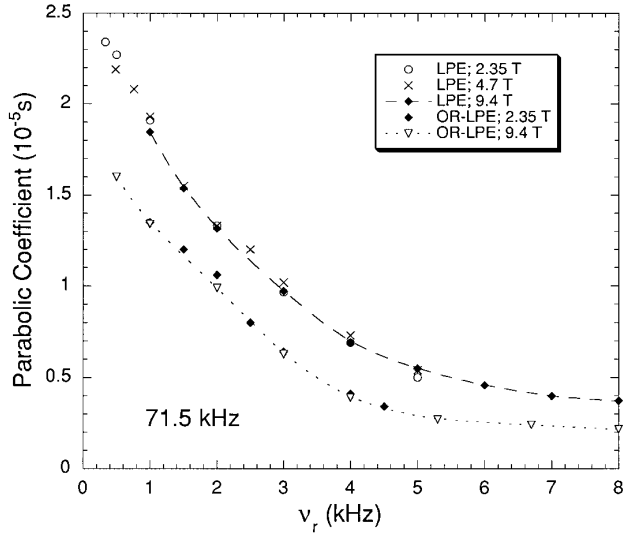

FIG. 6. Parabolic coefficients for LPE and OR-LPE as a function of ν_r at the different static fields given in the legend. There is no important B_0 dependence, as expected. The difference between the OR-LPE and LPE data at any given ν_r is indicative of the orbit-dependent dispersions of linewidth in the polycrystalline LPE sample. Lines are interpolated.

explicit reason to expect a dependence on B_0. Recognize, however, that in the sense that b is a strong function of ν_1^H, the very close agreement, in magnitudes, shown between the 9.4, 4.7, and 2.35 T LPE data sets is well within experimental error, given the stated uncertainty in the absolute ν_1^H calibration at each field. Second, even though the OR-LPE sample has smaller b's, relative to the LPE sample, for comparable conditions, the overall *shape* of the dependence of b on ν_r is similar.

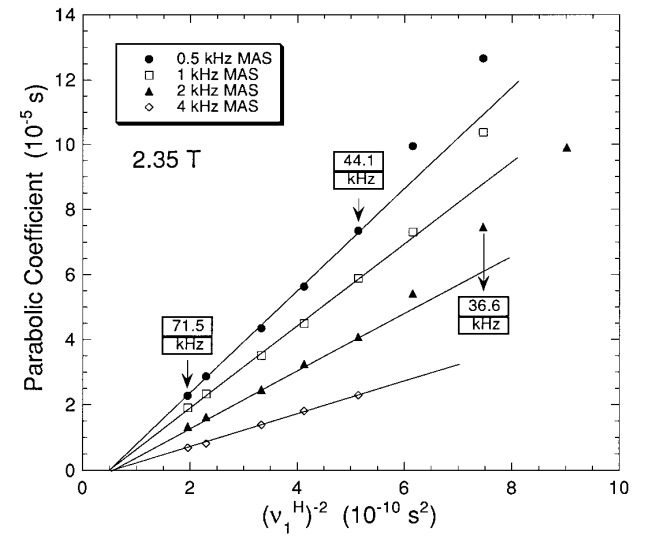

FIG. 5. Change of the parabolic coefficient, at 2.35 T, with the inverse squares of the RF field strengths for the various ν_r given in the legend. Certain values for ν_1^H are indicated by the arrows. Curves are reasonably linear for $\nu_1^H > 44$ kHz, as expected from the effective-field picture. However, extrapolation of the linear portions of these curves gives intercepts, short of the origin, in the vicinity of $\nu_1^H = 140$ kHz. We expected the intercept to be at the origin.

On-Resonance Linewidth Behavior

Figure 7 shows the dependence of linewidth on ν_1^H at 2 kHz MAS for both LW_n(obs) (see Fig. 7a) and its homogeneous contribution, $LW_n(T_2^C)$ (see Fig. 7b) as measured by the rotor-synchronized, single-echo pulse sequence. Data at static fields ranging from 1.4 to 9.4 T are included. Since the observed linewidth, is, among other things, a function of the inherent homogeneity of the magnet, a measure of this homogeneity is provided in the legend of Fig. 7a via the observed adamantane linewidth, LW(A). Note the different vertical scales for Figs. 7a and 7b.

Several qualitative deductions can be made, based on Fig. 7. First, the most striking observation is the strong dependence of LW_n(obs) on B_0. Note especially the increased ν_1^H dependence at higher B_0, a trend reflected in the $LW_n(T_2^C)$. Second, while there is a monotonic increase in the $LW_n(T_2^C)$ for LPE as a function of B_0 at any given ν_1^H, LW_n(obs) shows some non-monotonic behavior between 1.4 and 2.35 T, notwithstanding a consideration of the different adamantane LWs. Third, both the observed linewidth and its homogeneous contribution are smaller for OR-LPE than for LPE; while not shown, this is true for data at all values of B_0. Fourth, at lower values of ν_1^H, there is a very rapid increase in linewidth, similar to that reported previously for LPE (*4*), and it is strongly related to phenomena seen in other systems (*29*). This onset is most dramatic at lower B_0. At 2.35 T, this rapid increase in linewidth occurs for LPE

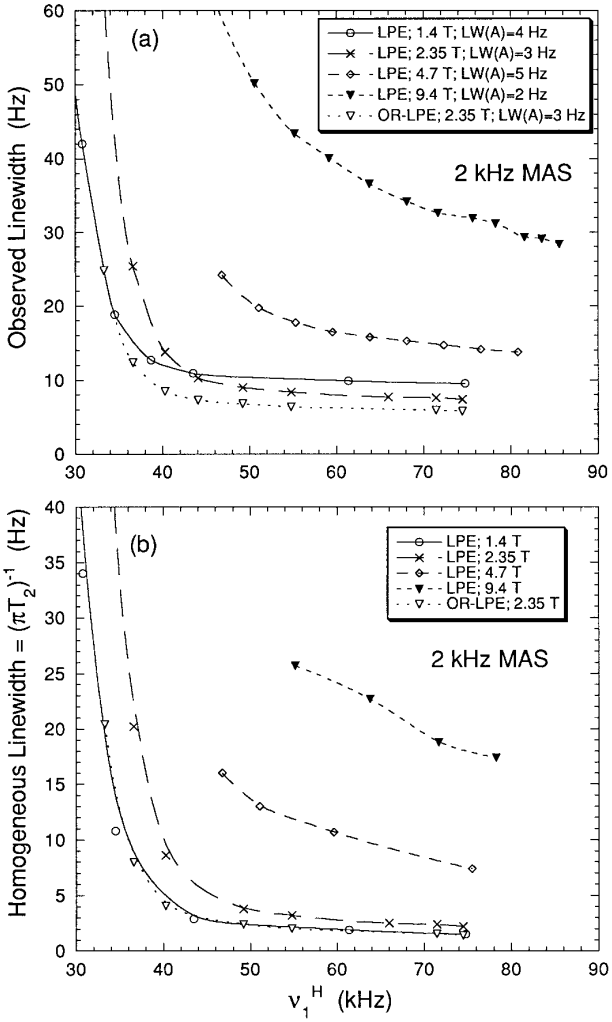

FIG. 7. Observed on-resonance linewidths (a) and their homogeneous contributions (b) at 2 kHz MAS as a function of ν_1^H for the various samples and B_0's given in the legends. Also in the legend in (a) is the observed linewidth, LW(A), for adamantane for a sample of the same size. Note the different vertical scales in (a) and (b) along with the strong dependence of both the observed linewidths and their homogeneous contributions on B_0. Note also the steep rise in linewidth at lower ν_1^H and the smaller linewidths associated with the OR-LPE carbons, relative to the LPE carbons under the same conditions. Lines are interpolated.

in the vicinity of $\nu_1^H = 40$ kHz and for OR-LPE about 4 kHz lower.

Prompted by ideas set forth in recent publications (*1, 2*), we use Fig. 8 as a test to determine whether the B_0 dependence in Fig. 7 can be understood in terms of, say, the chemical shift anisotropy (CSA) of the protons. In this scheme, the CSA would generate the necessity for irradiating the protons slightly "off-resonance," depending on rotor position. As discussed in the Introduction in connection with Eq. [3], the angular dependence of the CSA interaction, relative to, say, the fixed character of $\Delta\nu_{RF}$, changes the influence of MAS averaging in this problem. Nevertheless, even though the angular dependence is more complicated for the CSA case than for a fixed offset, a signature that off-resonance effects are important, even in the on-resonance case, is the fact that the $(\nu_1^H)^{-2}$ dependence, already seen for LW_f(ORPI) in Fig. 5, would be a characteristic common to both cases. In Figs. 8a and 8b such plots are shown for the 2 kHz MAS data of Fig. 7. Indeed there is a reasonably linear region for the higher ν_1^H values for all of the data sets. Moreover, the slope is a strong function of B_0. The linearity of these plots along with the strong B_0 dependence is a solid indication that an ORPI mechanism is partly responsible for the observed LWs. We thus define LW_n(ORPI) to be the portion of

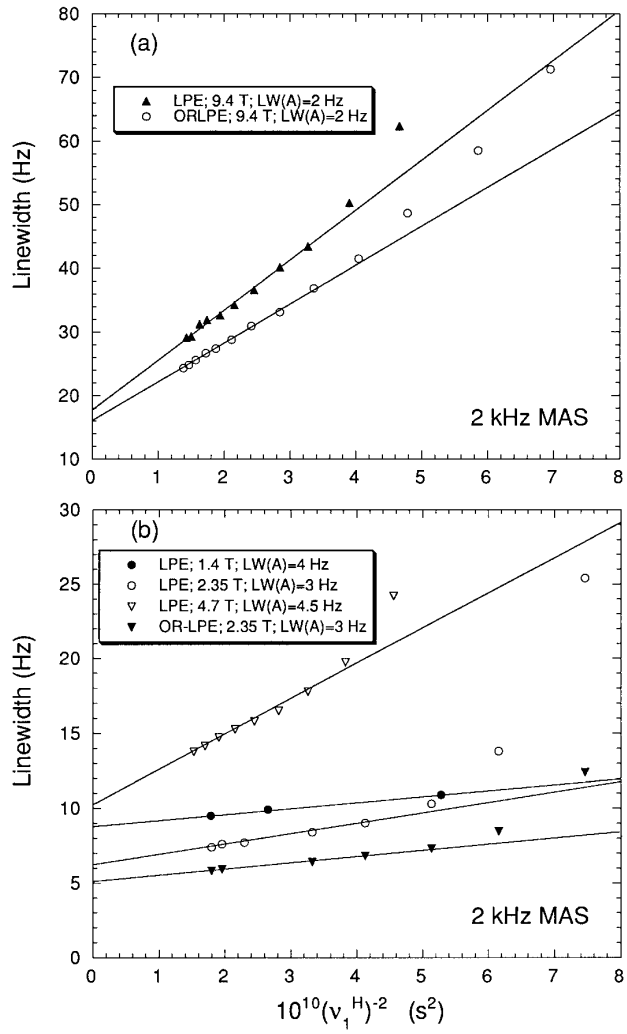

FIG. 8. Observed on-resonance linewidths at 2 kHz MAS plotted against the inverse square of the RF field strength for the samples and B_0 values given in the legends. The 9.4 T data have been plotted separately in (a) to allow a more favorable vertical scale for displaying data at the lower B_0 values in (b). Adamantane linewidths are included in the legend. As indicated, plots are quite linear at all B_0 values for ν_1^H above about 50 kHz; such behavior is very consistent with the effective-field picture. Ordinate intercepts in these samples should represent the non-ORPI contributions to linewidth, including static field inhomogeneity, plus whatever other T_2^C-based contributions are independent of ν_1^H. The latter contributions are less than 2 Hz in LPE.

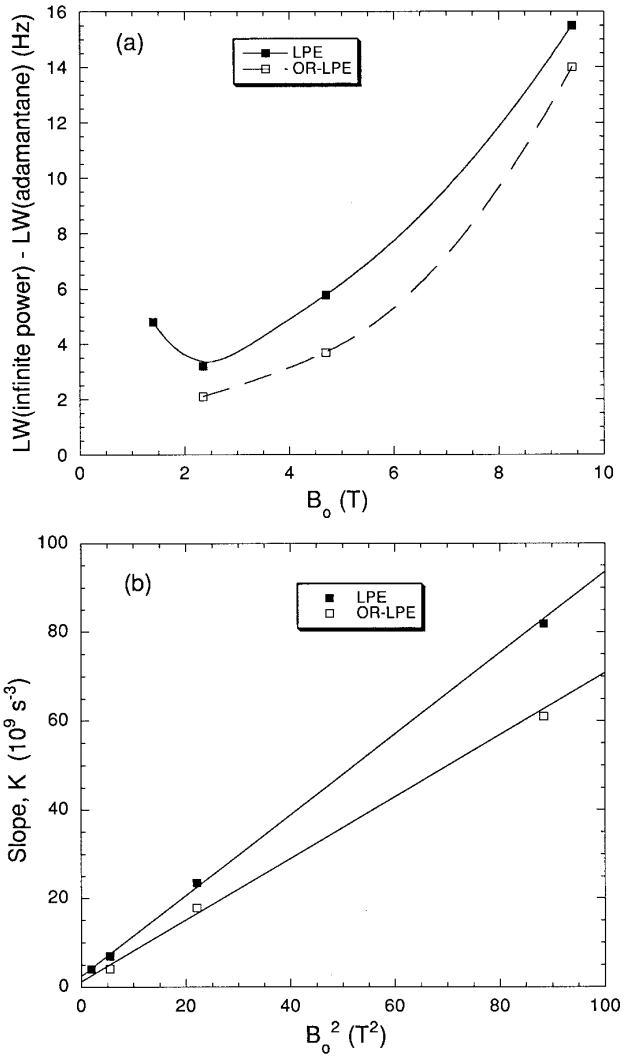

FIG. 9. Plots, based largely on the 2 kHz MAS data of Fig. 8, which examine the B_0 dependence of (a) the predominantly inhomogeneous contributions to linewidth, corrected for B_0 inhomogeneity and distributions of Bloch–Siegert shifts, and (b) the homogeneous contributions to linewidth which display a $(\nu_1^H)^{-2}$ dependence. The slopes (see Fig. 8) which are plotted in (b) capture the strength of the latter contributions at each B_0 value. The choice of B_0 as the abscissa in (a) is discussed in the text; linearity with B_0^2, illustrated in (b), is very strong evidence that the proton chemical shift anisotropy is mainly responsible for the B_0 dependences seen in Figs. 7 and 8.

the linewidth which depends on $(\nu_1^H)^{-2}$. The B_0 dependence of LW_n(ORPI) as well as the remaining portion of LW_n(obs) is the subject of Fig. 9.

In Fig. 9b, the slopes of the data of Fig. 8 (plus some slopes, not shown, for the OR-LPE sample) are plotted versus B_0^2. The linearity of this plot is very strong proof that the interaction which produces the off-resonance behavior is proportional to B_0 (Eqs. [2] and [4]). The proton CSA, therefore, becomes a very likely candidate for this interaction.

In Fig. 9a, we turn our attention briefly to the non-ORPI contribution to LW_n(obs). At least at 1.4, 2.35, and 4.7 T, the non-ORPI contribution is larger than the ORPI contribution. Plotted against B_0 is the difference between the intercept linewidths of Fig. 8 (the part of the linewidth which does *not* scale with $(\nu_1^H)^{-2}$) and the corresponding adamantane linewidths observed for a sample similar in size to the LPE sample. This difference should represent contributions from (a) T_2^C processes which are independent of ν_1^H; (b) inhomogeneous broadening arising from, say, any anisotropic magnetic susceptibility of LPE, distributions of isotropic carbon chemical shifts in the crystalline regions, and variations in the magic angle from sample to sample; and (c) second-order dipolar shifts (*13, 14*), which are very weak in adamantane owing to the fast rotation of each adamantane molecule on its lattice site. Contributions which are *excluded* from the difference linewidth of Fig. 9a include magnet inhomogeneity and contributions from RF inhomogeneity via Bloch–Siegert-shift (*30*) broadening. (Note that by assigning a fixed value to the adamantane linewidth, we are assuming that the Bloch–Siegert effects are negligible, a reasonable assumption as we will discuss later. For now, suffice it to say that such a contribution to line broadening depends on $(\nu_1^H)^2$; hence, if important, such a contribution should be very evident for the leftmost data points in Fig. 8. The data do not give evidence of such a contribution.)

The points in Fig. 9a do not show very linear behavior, especially for the point corresponding to a B_0 of 1.4 T. The choice to plot these difference linewidths against B_0 shows our bias that the most likely origin for this "excess LW" is inhomogeneous contributions arising from either anisotropic bulk magnetic susceptibility or distributions of isotropic carbon chemical shifts; both influences produce line broadening proportional to B_0. The non-monotonic behavior of the point at 1.4 T may well arise from second-order dipolar effects (*13, 14*) which are greatly amplified at lower B_0 values owing to their B_0^{-2} dependence. The importance of possible, ν_1^H-independent contributions to $LW_n(T_2^C)$, can be evaluated by subtracting LW_n(ORPI) values obtained from Fig. 8 or Fig. 9b from direct measurements of $LW_n(T_2^C)$ (Fig. 7b). Table 2 shows a breakdown of linewidth contributions, using one set of data at 2 kHz MAS at each value of B_0. In Table 2, $LW_n(\Delta T_2^C)$ is this ν_1^H-independent contribution to $LW_n(T_2^C)$; $LW_n(\Delta T_2^C)$ is small, i.e., close to 1 Hz, for the larger ν_1^H values, except at 4.7 T. At this time, we do not understand why this 4.7 T datum is unique; a repeat measurement gave the same result. Other measurements at 4.7 T, e.g., LW_n(ORPI) values, are not suspect in the sense that they fit the trends at the other B_0 values. Therefore, we conclude that T_2^C contributions from, say, fast librational modulation of the ^{13}C–^1H dipolar interactions, offer a very small (<2 Hz) contribution to linewidth. The variable-temperature, 8.4 T linewidth measurements cited under Experimental further support the insignificance of motional contributions to linewidth. Also, note that in Table 2, the last column, LW_n(inh) − LW(A), has a meaning closely related to the quantity plotted in the ordinate of Fig. 9a.

Having established the existence of the LW_n(ORPI) contri-

TABLE 2
Analysis of Different On-Resonance Linewidth Contributions (in Hz) for One Set of LPE Data at 2 kHz MAS and Four B_0 Values

B_0 (T)	ν_1^H (kHz)	$LW_n(obs)^a$	$LW_n(T_2^C)^b$	$LW_n(ORPI)^c$	$LW_n(\Delta T_2^C)^d$	$LW(inh)^e$	$LW(inh) - LW(A)^f$
1.4	74.8 (30)	9.5 (1)	1.5 (1)	0.7 (1)	0.8 (2)	8.0 (4)	4.0 (6)
2.35	74.5 (20)	7.4 (1)	2.2 (1)	1.3 (1)	0.9 (2)	5.2 (2)	2.2 (3)
4.7	75.5 (20)	14.3 (2)	7.4 (3)	4.1 (4)	3.1 (7)	6.9 (5)	2.4 (7)
9.4	84.1 (25)	29.1 (4)	14.3 (8)	13.1 (10)	1.2 (18)	14.8 (12)	12.8 (15)

Note. Full-range error estimates, in units of the last decimal place, are given in parentheses.
[a] Observed linewidth (LW).
[b] LW from measured T_2^C; $[=(\pi T_2^C)^{-1}]$.
[c] Portion of LW dependent on $(\nu_1^H)^{-2}$ (from Figs. 8 and 9b).
[d] The ν_1^H-independent T_2^C-contribution to LW $(=LW_n(T_2^C) - LW_n(ORPI))$.
[e] Inhomogeneous LW $(=LW_n(obs) - LW_n(T_2^C))$.
[f] Portion of LW(inh) not accounted for by observed adamantane LW (LW(A)).

bution and its rather simple behavior at higher values of ν_1^H at 2 kHz MAS, we now turn to a closer inspection of the behavior of $LW_n(obs)$ as a function of ν_r, paying particular attention to the behavior at lower values of ν_1^H.

Figures 10a and 10b, respectively, present 2.35 and 9.4 T data for $LW_n(obs)$ as a function of ν_1^H for several different values of ν_r which range from 0.5 to 5 kHz at 2.35 T and from 1 to 8 kHz at 9.4 T. Note the difference in vertical scales. One plot for OR-LPE is also shown to illustrate the generally narrower linewidths of OR-LPE relative to LPE as well as the implied existence of distributions of linewidths embodied in the LPE measurements. Two observations are especially noteworthy in Fig. 10. First, for LPE, in the range of ν_1^H characterized by strong changes in $LW_n(obs)$, the values of ν_1^H, at which comparable linewidths are observed, increase about 2 kHz (at 2.35 T) and about 3 kHz (at 9.4 T) for every 1 kHz increase in ν_r. This pattern is quite regular above a ν_r of 2 kHz at 2.35 T and above 4 kHz at 9.4 T; below those values the change of ν_1^H with ν_r is not as fast. Second, compared to the off-resonance case where $LW_f(ORPI)$ was often dominant and where this contribution underwent a nearly fourfold reduction as ν_r changed from 1 to 5 kHz (see Fig. 6), the sensitivity to ν_r of $LW_n(obs)$ at the higher values of ν_1^H is considerably diminished.

Figure 11 displays the same kind of data as Fig. 10, except that it does so in a way which may reflect the spectroscopist's parameter choices more realistically; i.e., spinning speed may be chosen as a variable in setting up an experiment more often than ν_1^H. This plot shows the behavior of $LW_n(obs)$ as a function of ν_r for various choices of B_0 and ν_1^H. At higher values of ν_1^H, e.g., 71 kHz at 2.35 T, 69 kHz at 4.7 T, and 72 kHz at 9.4 T, $LW_n(obs)$ is rather flat, or even slightly decreasing, in the range of ν_r from 1 to 5 kHz; relative flatness from 1 to 8 kHz requires a ν_1^H of 83 kHz at 9.4 T. (Historically, it was this ν_r-insensitive behavior, in contrast to the ν_r-sensitive behavior of $LW_f(obs)$, which puzzled us and caused us to set aside our reporting of most of these data. We knew of the strong B_0 dependence of $LW_n(obs)$ and were suspicious that the proton CSA played a significant role. Nevertheless, we did not examine this problem in sufficient detail.) Figure 11 illustrates two other points, namely, (a) that in the range of ν_r between 1 and 2 kHz, there is often a noticeable linewidth decrease which may be associated with some MAS averaging, and (b) that increasing ν_r with insufficient ν_1^H can ruin resolution.

DISCUSSION

The data just presented relate to linewidths in a strongly coupled spin system. There are many facets to the question of resolution, and we are exploring a limited area in this paper. In presenting this work, we had these guiding perspectives: First, if one wishes to improve resolution, one must understand well, not only the mechanisms of line broadening but also the role that proton spin fluctuation rates play. Certain strategies for applying non-CW decoupling are designed to produce a second kind of averaging which competes against, or is intended to dominate, the spin fluctuations (*1*). Therefore, we will attempt to gain insight into the rate of spin fluctuations. Second, LPE, we believe, is a material which has reasonable generality. We anticipate that the LPE data reported herein represents the general behavior of *a methylene carbon with natural abundance enrichment in a relatively rigid aliphatic solid where protons are the only other magnetic nuclei.* The role, as we shall see, that proton CSA plays in the determination of on-resonance linewidths as well as the very limited role that bulk magnetic susceptibility anisotropy plays will be typical of aliphatic solids. Also typical is the extent of proton couplings and the rate of spin fluctuations. Many of the mechanisms discussed here will also carry over to methylene carbons in other organic environments even though spin fluctuation rates may be slower and susceptibility anisotropy may become more important. Third, it is not so much our intent in this discussion to present a lot of mathematical detail as it is to understand the

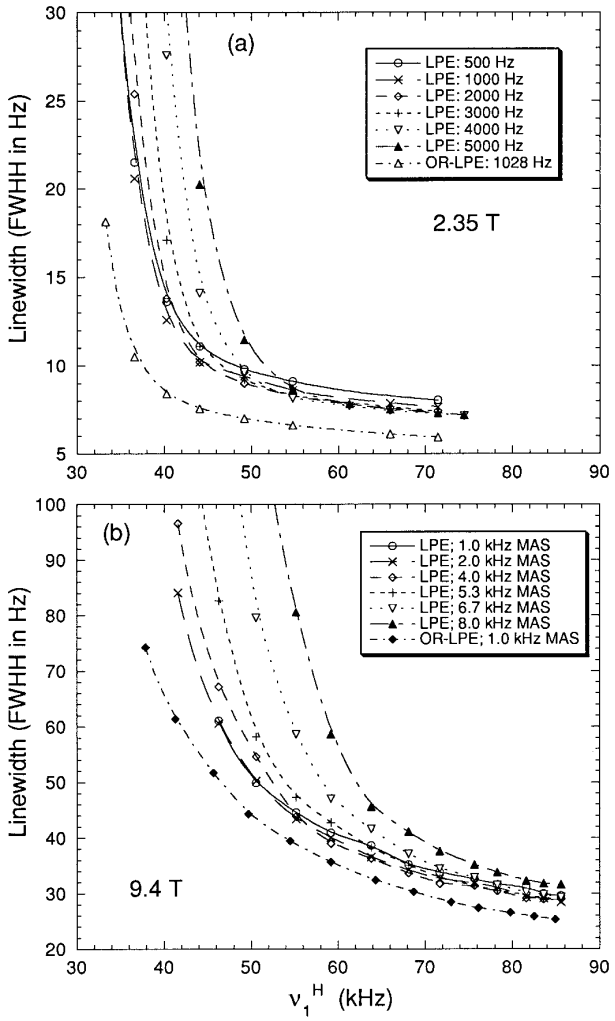

FIG. 10. Observed on-resonance linewidths at 2.35 T (a) and 9.4 T (b) as a function of RF field strength for the various samples and ν_r values given in the legends. Note the different vertical scales and the fact that in the region of smaller ν_1^H, the ν_1^H where a given strong broadening occurs is (1) lower by about 4 kHz for OR-LPE versus LPE and (2) increases with increasing ν_r. This strong broadening is attributed to MAS-assisted dipolar fluctuations (MADF). This broadening goes from modest to dominant over a relatively small range of ν_1^H. Also, $(\delta\nu_1^H/(\delta\nu_r)$ at a constant linewidth of, say, 25 Hz in (a) or 90 Hz in (b), is about 2 above $\nu_r = 2$ kHz in (a) and about 3 above $\nu_r = 4$ kHz in (b). The MADF influence on linewidth along with the ORPI effects illustrated in Figs. 7–9 suggests the use of large ν_1^H for achieving good resolution at higher B_0, especially if one is inclined to increase ν_r proportionally with B_0. Lines shown are interpolated.

phenomenology so that one can avoid, or intelligently make use of, certain characteristics of line broadening.

Off-Resonance Behavior

As previously mentioned, the behavior of LW_f(obs) is fairly standard (*4, 8, 9*) insofar as Eq. [5] is obeyed. What was more intriguing to us was the ν_r dependence of the parabolic coefficient in Eq. [5] (see Figs. 4 and 6). From a practical standpoint, the data suggest that fast spinning is desirable since, in general, a sample has different kinds of protons and one must choose a decoupling frequency, somewhat off-resonance for each kind of proton. In Fig. 6, the parabolic coefficient monotonically decreases at least to $\nu_r = 8$ kHz; for all of our observations, faster spinning always led to a further reduction of LW_f(ORPI).

In the effective field picture of Fig. 1 and for larger ν_1^H, $\langle I_{zi}\rangle$ is simply scaled by $(\Delta\nu_{off}/\nu_1^H) \approx (\Delta\nu_{RF}/\nu_1^H)$, thereby giving LW_f(ORPI) in Eq. [4] its dependence on $\Delta\nu_{RF}^2$ and $(\nu_1^H)^{-2}$. From Figs. 3 and 5, this effective field picture seems to be a decent approximation, at least for $\nu_1^H > \approx 47$ kHz (albeit the convergence of the intercepts in Fig. 5 to a point short of the origin remains puzzling).

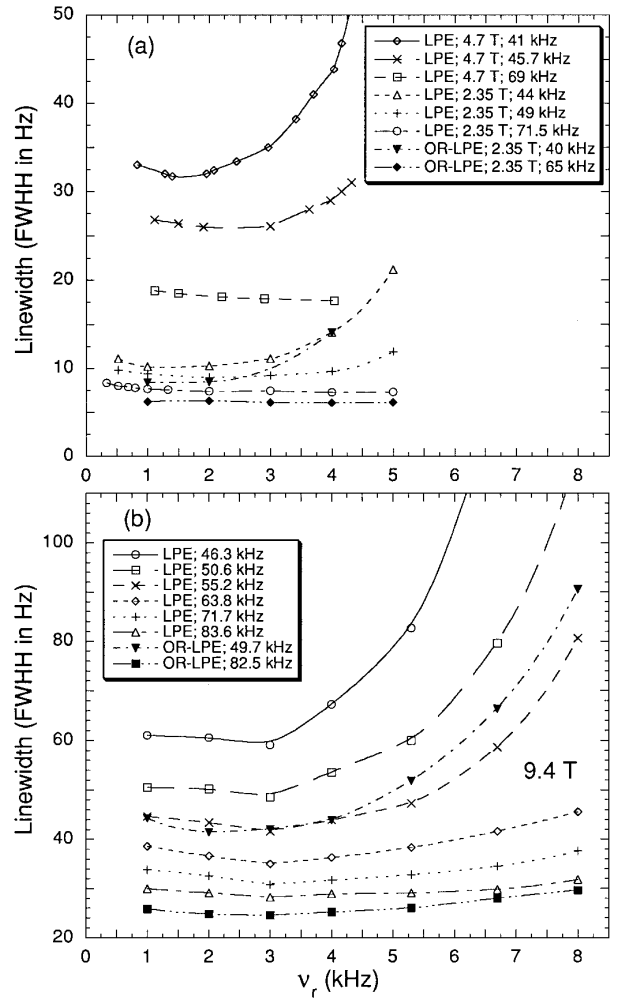

FIG. 11. Observed on-resonance linewidths at the lower B_0's (a) and at 9.4 T (b) as a function of ν_r for the samples and ν_1^H values in the legends. Note the different vertical scales. The strongly increasing linewidths at higher ν_r for the lower ν_1^H values reflect the onset of MADF broadening. The relative insensitivity to ν_r at higher ν_1^H is a result of the $J(0)$ term in the expression for LW(ORPI) in Eq. [10]. The flatness also suggests that, for ν_r up to 8 kHz in polyethylene, spinning does not significantly alter the rate of dipolar fluctuations. Lines shown are interpolated.

While experimental data closely adhere to Eq. [5], thereby underscoring the presence of spin fluctuations in producing broadening (and the validity of a general expression like Eq. [4]), the decrease in the parabolic coefficient, b, at higher ν_r values is better understood from the "static-spin" representation of Eq. [3]. There it is evident that MAS will coherently eliminate splittings associated with any isochromat since $\Delta\omega_s$, in the off-resonance case where $\Delta\omega_{off} = \Delta\omega_{RF}$, has the simple angular dependence of ω_{Di}. In other words, the observed dependence of b on ν_r is evidence that the coherent averaging arising from faster spinning is moderating the broadening influence from the more random spin fluctuations; the implication is that characteristic times for rotation and for spin fluctuations are becoming comparable.

We now write down a couple of equations with the sole purpose of seeking information about the important issue of the time scale of the spin fluctuations. For an axially symmetric tensor, such as the dipolar tensor, the angular dependence in, say, Eq. [1], can be rewritten (*31*), in the presence of MAS, as

$$(1 - 3\cos^2\theta_i) = A_{ic}\cos(\omega_r t) + A_{is}\sin(\omega_r t) + B_{ic}\cos(2\omega_r t) + B_{is}\sin(2\omega_r t), \quad [6]$$

where the constants are functions of β_i and α_i, respectively the polar and azimuthal angles of the ith ^{13}C–^{1}H vector in the rotor frame. Equation [6] simply states that ω_{Di} has a trajectory, under MAS, which is the sum of terms that fluctuate at ω_r and $2\omega_r$. Therefore, we anticipate that in the simple picture represented by Eq. [4], T_{2f}^{C}(ORPI) will depend on $J(\omega_r)$ and $J(2\omega_r)$, not $J(0)$. If we postulate (a) that the proton quantization is determined by the effective field picture, (b) that the rate of proton spin fluctuations in any given orbit is not dependent on rotor position, and (c) that the only important term contributing to $T_{2f}^{C}(\mathrm{ORPI})^{-1}$ is the dipolar term of Eq. [1], then we can write the following expression for $T_{2f}^{C}(\mathrm{ORPI})^{-1}$,

$$T_{2f}^{C}(\mathrm{ORPI})^{-1} = \sum_i [(\mu_0/4\pi)(\gamma_C\gamma_H\hbar/r_i^3)(\Delta\nu_{RF}/\nu_1^H)]^2 \times [I(I+1)/12][A_i^2 J(\omega_r) + B_i^2 J(2\omega_r)]. \quad [7]$$

In Eq. [7], $J(n\omega_r)$ is the reduced spectral density for the proton spin fluctuations and $A_i^2 = 2\sin^2 2\beta = A_{ic}^2 + A_{is}^2$ and $B_i^2 = \sin^4\beta = B_{ic}^2 + B_{is}^2$. The α dependence of the A and B coefficients of Eq. [6] can be eliminated because $T_{2f}^{C}(\mathrm{ORPI})^{-1}$ depends only on the β-dependent path of a particular orbit; α determines only the position along a particular path.

It is obvious from Eq. [7] that if the assumptions giving rise to this equation are appropriate, there will be a lot of heterogeneity in the T_{2f}^{C}(ORPI)'s of carbons belonging to different orbits owing to the range of A_i^2 and B_i^2 values. Nevertheless, we could approximate an average $T_{2f}^{C}(\mathrm{ORPI})^{-1}$ for LPE in Eq. [7] by replacing these two quantities by their isotropic averages, respectively, (16/15) and (8/15). In contrast, for OR-LPE we have only a single orbit to consider ($\beta = \pi/2$) for the two dominant attached protons, and the only nonzero coefficient is $B_i^2 = 1$.

Equation [7] applied to the OR-LPE sample offers a very simple way to examine the spin correlation function because both ^{13}C-bonded protons have the same orbit for ^{13}C–H dipolar interactions and because one is dealing only with the spectral density at $2\omega_r$. In this simple picture, the dependence of b on ν_r for the OR-LPE data in Fig. 6 is exactly that of the orbit-averaged spectral density function, $J(2\omega_r)$. We digress briefly to discuss the form of $J(\omega)$.

The mathematical form of the spectral density function, $J(\omega)$, associated with fluctuations of the proton spins along their quantization axis is sometimes (*8, 32*) described as arising from a Lorentzian correlation function of the form $(1 + \tau^2/\tau_s^2)^{-1}$, in which case $J(\omega)$ is given by an exponential function of the form

$$J(\omega) = \pi\tau_s\exp(-|\omega|\tau_s). \quad [8a]$$

Equation [8a] has been found (*32*) to describe very well the cross-polarization rates in cubic CaF_2 when an RF field of amplitude ν_1^{Ca} is applied in the presence of ^{19}F nuclei which have taken on dipolar order via adiabatic demagnetization in the rotating frame. These CP rates are closely related to $J(\omega)$, the spectral density of the ^{19}F spin fluctuations along B_0. Admittedly, other analyses (*33*) of these same data, based on Gaussian memory functions (related to the correlation functions), give similarly good agreement with experiment. The $J(\omega)$'s pertinent to Eq. [7] similarly describe spin fluctuations along quantization axes, this time in the rotating frame. Again we rely on the effective time dilation by a factor of 2 in the rotating frame, relative to the laboratory frame, in the presence of a strong, resonant ν_1^H. The *shape*, or functional dependence, of the spectral density functions in the two frames should be the same for any given substance.

For LPE, we do not necessarily expect the spectral density to be described by Eq. [8a] since the LPE lattice is not cubic and since there are fewer strongly interacting protons around each carbon than there are strongly interacting ^{19}F nuclei around each ^{43}Ca nucleus in CaF_2. The latter feature helped to rationalize the Lorentzian form of the correlation function (*8*). Nevertheless, experimental evidence (*25*) of an exponential spectral density function in LPE has been given for static LPE samples in the regime of larger ω. Here we are dealing with the regime of smaller ω; hence we wish to keep an open mind as to the shape of the spectral density function at lower ω. Thus, more from the point of view of computational simplicity than from particular physical insight, we also considered a Lorentzian spectral density of fluctuations,

$$J(\omega) = 2\tau_s/[1 + (\omega\tau_s)^2]. \quad [8b]$$

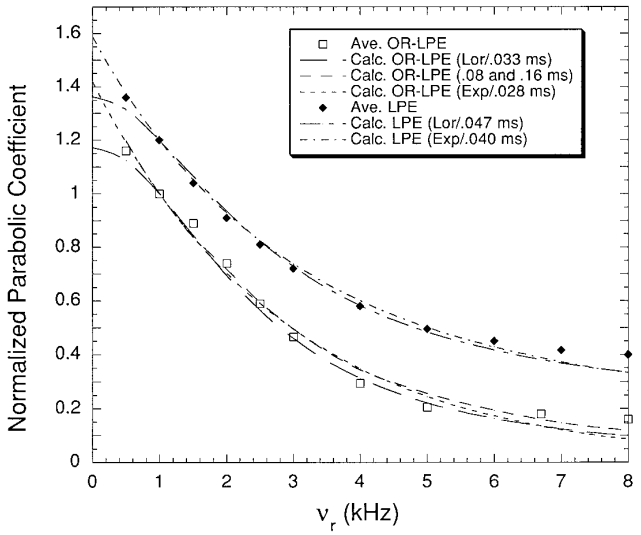

FIG. 12. Attempts to fit the shape (not the magnitude) of the LPE and OR-LPE data of Fig. 6. The experimental data represent averages of the parabolic coefficient, for $\nu_1^H = 71$ kHz, taken at the various B_0's for each sample. The calculated curves consider only the fluctuations of the two attached methylene protons; four of the five calculated curves given in the legend are based on Eq. [7] using $B_i = 1.0$ for the OR-LPE and $A_i = 16/15$, $B_i = 8/15$ for LPE. "Lor" in the legend refers to the Lorentzian spectral density function of Eq. [8b] and "Exp" refers to Eq. [8a]. Correlation times, τ_s, are also given in the legend. The OR-LPE calculation with 2 times is the two-lifetime Monte Carlo calculation described in the text where the numbers correspond to shorter spin-state lifetimes for mutual spin flips between the $^{13}CH_2$ pair of protons and longer spin lifetimes associated with a flip with another, more distant proton. The most obvious difference between the calculated curves is the more peaked amplitude at $\nu_r = 0$ for the exponential spectral density; although the 2-lifetime model (whose curve extends only to $\nu_r = 0.5$ kHz) generates a steeper rise at lower ν_r compared to its Lorentzian, single-lifetime counterpart. The data support a steeper rise at low ν_r than would be predicted by the single-lifetime Lorentzian fits. At higher ν_r, data decrease more slowly than any of the calculations predict. Normalization of the data to the calculated curves is such that at $\nu_r = 1$ kHz the experimental data are scaled to agree with the calculated values and both are set to 1.0. *The LPE data along with the calculated curves are displaced vertically by 0.2 for clarity.*

This spectral density would pertain to an exponential correlation function associated, for example, with random, sudden spin-state changes of those protons attached to the ^{13}C nuclei. Such a model ignores any possible slower fall-off of the correlation function as a result of the conservation of total local polarization. Recall that it is not the focus of this paper to analyze spin-correlation functions in detail. Rather, our goal is to come to an approximate assessment of the spin lifetimes so that we can comment further on the time scales available for implementing decoupling schemes like TPPM.

Figure 12 shows our attempt to use Eq. [7] to match the *shapes* of both the OR-LPE and the LPE curves of Fig. 6 (the parabolic coefficient is proportional to $T_{2f}^{C}(\mathrm{ORPI})^{-1}$) by varying τ_s in Eqs. [8a] and [8b]. We considered only the spin fluctuations of the two bonded methylene protons, assuming these fluctuations were uncorrelated. The calculated and experimental curves are normalized to agree for $\nu_r = 1$ kHz. For the LPE calculation, we used the isotropic averages for A_i and B_i. The best fits we could obtain are $\tau_s = 33$ and 47 μs for the OR-LPE and the LPE, respectively, using Eq. [8b]; 28 and 40 μs were the corresponding best fits using Eq. [8a]. The spin-state lifetimes, recall, should be about twice τ_s. The fits are modestly good considering the crudeness of the models, but neither spectral density function predicts well the slower rate of decrease of the experimental data at the higher ν_r, even though Eq. [8b] falls off more slowly than [8a] with increasing ω.

In the Introduction, we raised the point that there may be a local bias to the spin correlation function whereby the tails of the correlation function might decay quite slowly (and its spectral density be quite peaked at $\omega = 0$) owing to the polarization–conservation aspect of the spin fluctuations. The slower decay of the Lorentzian correlation function and its exponential spectral density (Eq. [8a]) preserve these ideas better than the alternate functions considered here. Thus, the fits in Fig. 12 based on the spectral densities of Eq. [8a] are more peaked at small values of ν_r relative to the fits based on Eq. [8b]. If we look at the trends in the experimental OR-LPE and LPE data in Fig. 12 at lower ν_r, Eq. [8a] seems to fit better. As noted, however, Eq. [8b] describes the weaker rate of decrease of b with ν_r slightly better at larger ν_r. Hence, the data do not fully endorse either the exponential or the Lorentzian spectral densities. The estimates of τ_s, using both the exponential and the Lorentzian spectral densities, give modest agreement. Moreover, the τ_s of 48 μs for non-spinning OR-LPE (*25*) at high ω is not necessarily in conflict with the 28 and 33 μs values determined for OR-LPE in Fig. 12, given the different orientations represented and the fact that fluctuations arising from proton spin flips within the $^{13}CH_2$ group only contribute to the spinning OR-LPE data.

One measure of whether we have captured the appropriate physics is our ability to predict the magnitude of $T_{2f}^{C}(\mathrm{ORPI})^{-1}$ as well as its shape for the simplest case, OR-LPE. The $T_{2f}^{C}(\mathrm{ORPI})$'s calculated from Eq. [7], considering only the two bonded protons, translate into b values which account for 65–70% of the experimental b values over the range of ν_r from 0.5 to 5 kHz when $\tau_s = 33$ μs ($J(\omega)$ Lorentzian), the value of τ_s that gave the best fit to the shape of the curve in Fig. 12. For $\tau_s = 28$ μs ($J(\omega)$ exponential) the predicted b values were about 75–85% of experimental values over the 0.5 to 5 kHz range of ν_r. We then explored the possibility that the inclusion of more distant protons in the sum in Eq. [7] could close the gap between experiment and calculations. Inclusion of the four next-nearest protons at 0.214 nm gave a 10% increase in $T_{2f}^{C}(\mathrm{ORPI})^{-1}$, thereby reducing the discrepancy to a shortfall of about 25% for the Lorentzian function and about 12% for the exponential spectral density. We then looked at the range and numbers of more distant protons and concluded that a consideration of all protons could account for no more than a 15% increase over the $T_{2f}^{C}(\mathrm{ORPI})^{-1}$ calculated for the two bonded protons only. Hence, although we have not done this much larger calcu-

lation, the full exponential spectral density function should account for about 90% of the experimentally observed b values over the 0.5 to 5 kHz range of ν_r, whereas the Lorentzian should account for about 80%. Both functions, therefore, give reasonable agreement, with Eq. [8a] slightly superior. This outcome is probably satisfactory in view of the crudeness of the model, especially in that the spin fluctuations are simply included as a "property" of each spin, regardless of the couplings of the protons to one another. (Incidentally, the parallel calculations including only the two bonded protons of LPE and using the "isotropic-average" coefficients in Eq. [7] yield values of b which *over*estimate the experimental values by about 10–20% for $J(\omega)$ Lorentzian and $\tau_s = 47$ μs; overestimates range from 25 to 40% for $J(\omega)$ exponential and $\tau_s = 40$ μs.)

This leads us to the other computation of $J(\omega)$ that we tried, pertinent only to OR-LPE. Our principal reason for questioning the foregoing spectral density functions was that these functions should also predict the LW_n(ORPI) for on-resonance decoupling. Such predictions fell short by factors of 2 to 3. The discussion of on-resonance linewidths will be taken up shortly. However, as part of the discussion of the form of $J(\omega)$, we include a description of this modified calculation.

We started from the premise that the weakest assumption embodied in Eq. [7] was the claim that each spin fluctuated independently. Thus, we ignored the possibility that strong intramethylene proton–polarization–exchange events (mutual spin flips) could occur whenever the total I_z ($=I_{z1} + I_{z2}$) was zero. In an attempt to include this effect of mutual spin flips, we set up a Monte Carlo calculation for computing the mean square phase loss for the OR-LPE carbons during an integral number of rotor cycles. The times between spin flips were determined by a random number generator and the effective-field scaling of Eq. [3] was again employed. The overall correlation function, then, is the superposition of a Lorentzian correlation function plus a second, broader Lorentzian correlation function which is turned on only when I_z is zero. As a control for testing the Monte Carlo method for computing $T^C_{2f}(\text{ORPI})^{-1}$, we duplicated, within the approximately 5% statistical error of our calculation, the $T^C_{2f}(\text{ORPI})^{-1}$ values of Eq. [7] when the two spins were allowed to fluctuate independently with only one correlation time. Then, to model the case where mutual spin flips could occur, we set up the situation where, in addition to independent spin flips which would constantly occur with a longer lifetime, τ_{lg}, a second shorter lifetime, τ_{sh}, governing the rate of mutual spin flips, was invoked whenever the total I_z was zero. Whenever I_z was zero, the random number generators determining the τ_{lg} and the τ_{sh} state changes acted in parallel; thus, the inverse of the effective lifetime of each spin in this $I_z = 0$ state is $(\tau_{lg}^{-1} + \tau_{sh}^{-1})$. The result of these calculations for OR-LPE was that a fit very similar to the others shown for OR-LPE in Fig. 12 was obtained with parameters having $\tau_{lg} = 160$ μs and $\tau_{sh} = 80$ μs. (To relate these parameters to the earlier result with $\tau_s = 33$ μs and a lifetime of 66 μs, this more complex model yields an effective lifetime in the $I_z = 0$ state of 53 μs while the lifetime in the $I_z = \pm 1$ states is 160 μs.) For OR-LPE it is a feature of the geometric terms that for the *off*-resonance case, the mean square phase loss accumulates more quickly when $I_z = 0$ than when $I_z = \pm 1$; hence the fit to the experimental data depends more strongly on τ_{sh} than on τ_{lg}. As a result, the fit is not very sensitive to modest changes in τ_{lg}. Also, for $\nu_r \geq 1$ kHz, the b values, using this two-lifetime model, agreed to within 5% with those calculated from the single-lifetime Lorentzian fit; significant relative increases in b for the two-lifetime model were only seen below $\nu_r = 1$ kHz. The relative importance of the lifetimes in the $I_z = 0$ or $I_z = \pm 1$ states for contributing to mean square phase loss depends on the dispositions of the two methylene protons and the value of n for different $J(n\omega_r)$. Thus, in LPE, some isochromats will have T^C_{2f}(ORPI)'s strongly influenced by τ_{lg} and others, as is in the case of OR-LPE, will be strongly influenced by τ_{sh}. *Therefore, if there is indeed a disparity in the effective lifetimes of the $I_z = 0$ and the $I_z = \pm 1$ states, owing to intramethylene mutual spin flips, then the orientation-dependent dispersion in $T^C_{2f}(\text{ORPI})^{-1}$ could be significantly larger than that indicated by the range of coefficients in Eq.* [7].

In the foregoing exercises for extracting spin lifetimes from plots like those of Fig. 6, we have made the implicit assumption that up to $\nu_r = 8$ kHz, ν_r is not influencing τ_s. Other authors have invoked such a dependence to explain their observations, e.g., in ferrocene (*34*). Ferrocene has much weaker, motionally averaged proton–proton couplings, so it is more reasonable that ν_r influence τ_s. If fluctuations in LPE were a function of ν_r, then fluctuations should slow down as ν_r increases, thereby making MAS averaging even more effective at the higher ν_r values. This should accelerate the decrease of b with ν_r at higher ν_r; a retardation is observed relative to the Lorentzian and exponential forms of $J(\omega)$ considered. Thus, LW_f(obs) data do not suggest a lengthening of τ_s with ν_r in LPE up to $\nu_r = 8$ kHz. We will also give an argument later, based on "on-resonance" data, suggesting that there is little, if any, slowdown in spin fluctuation rates up to $\nu_r = 8$ kHz.

Before we leave the discussion about off-resonance line broadening we reiterate the fact that the off-resonance data have offered some insight into the time scale of the proton spin fluctuations. Implicitly we have assumed that these fluctuation rates are not affected by modest (up to 3 kHz) departures from resonance, when ν_1^H is at least 15–20 times bigger than these offsets. Similarly, what we learned about spin fluctuations should also be applicable to the way in which spin fluctuations are invoked to explain the *on-resonance* linewidths.

On-Resonance Behavior

Figures 8 and 9 together establish that, for $B_0 \geq 1.4$ T, LW_n(ORPI), which is defined to be the part of the LW_n(obs) which shows the $(\nu_1^H)^{-2}$ behavior, is very nearly proportional

to B_0^2. Moreover, $LW_n(T_2^C)$ usually exceeds $LW_n(ORPI)$ by less than 2 Hz; in other words, $LW_n(ORPI)$ and its B_0^2 dependence are traceable to a T_2^C process. Recognizing that the general form for $T_2^C(ORPI)^{-1}$ is the product of the square of some interaction strength times some linear combination of spectral density functions, we look for an interaction, linear in B_0, to give rise to $LW_n(ORPI)$.

As mentioned in the Introduction, such a candidate interaction has already been discussed in other publications (*1, 2, 4*). This interaction is the proton chemical shift anisotropy (CSA). The corresponding "interaction strength" appropriate to LW(ORPI) takes the form given in Eq. [3]. This expression involves the product of the ^{13}C–^1H dipolar interaction and the proton CSA. The existence of a CSA means that most of the time, the protons are being irradiated slightly off-resonance since, at best, the choice of RF frequency matches the resonance defined by the isotropic proton chemical shift. Using Eq. [3], this is equivalent to making the substitution

$$\Delta\omega_{off}(i) = \Delta\omega_{CSA}(i) = [\gamma_H B_0(\sigma_\parallel - \sigma_\perp)/3](1 - 3\cos^2\theta_{ci}), \quad [9]$$

where $(\sigma_\parallel - \sigma_\perp)$ is the difference, taken to be 6.9 ppm for LPE (*35*), between the parallel and perpendicular components of the chemical shift tensor, assumed axial. Moreover, the unique axis of this tensor, presumed to lie along the C–H bond, makes the angle θ_{ci} with B_0; hence, for the two bonded protons in LPE, θ_{ci} is the same as θ_i in Eq. [1], which defines ω_{Di}. In order to develop a proper $T_{2n}^C(ORPI)^{-1}$ expression appropriate for MAS, using assumptions parallel to those used to develop Eq. [7], the angular terms in each product, $\Delta\omega_{off}(i)\omega_{Di}$, must be expressed in terms of their ω_r dependence. If we restrict our attention to the dominant contributions from the two bonded methylene protons, then we must analyze the ω_r dependence of $(1 - 3\cos^2\theta_i)^2$. Squaring the expression in Eq. [6] and using trigonometric identities reveal that for the general isochromat, one has sine and cosine terms oscillating at $n\omega_r$ for $n = 0$, 1, 2, 3, and 4. Correspondingly, spectral densities, $J(n\omega_r)$ at each of these frequencies will be involved in the expression for $T_{2n}^C(ORPI)^{-1}$. Rather than write down these rather tedious expressions, we choose to deal quantitatively only for the case of OR-LPE, where $(1 - 3\cos^2\theta_i)$ for the bonded methylene protons can be replaced by $\cos[2(\omega_r t + \psi_i)]$ for all ^{13}C nuclei in the sample and ψ_i is a phase factor. The square of the latter term is simply $\{0.5 + 0.5\cos[4(\omega_r t + \psi_i)]\}$; hence, the corresponding relaxation expression will involve only $J(0)$ and $J(4\omega_r)$. That expression, adding the effects of both ^{13}C-bonded protons, is

$$T_{2n}^C(ORPI)^{-1} = [(\mu_0/4\pi)(\gamma_C\gamma_H\hbar/r_i^3) \times (\sigma_\parallel - \sigma_\perp)(\gamma_H B_0/\omega_1^H)]^2 \times [I(I+1)/216][2J(0) + J(4\omega_r)]. \quad [10]$$

The fact that $\Delta\omega_{off}(i)\omega_{Di}$ includes a "constant" term, giving rise to the $J(0)$ term in Eq. [10], means that ν_r will have no influence on this term until ν_r becomes fast enough to effect a slowing of the spin fluctuation rate. Also, this $J(0)$ term will, in principle, be sensitive to any long tails which the spin correlation function may possess. At least for the OR-LPE sample it is now apparent why the on-resonance linewidth had very little sensitivity to ν_r. $J(0)$ is always larger than $J(4\omega_r)$; moreover, since the OR-LPE data of Fig. 6 reflects $J(2\nu_r)$ versus ν_r, we can see that $J(0) \geq J(1\text{ kHz}) \approx 4J(8\text{ kHz})$. Hence, $J(0) \geq 4J(4\omega_r)$ already at $\nu_r = 2$ kHz. Therefore, the ν_r-independent $J(0)$ term dominates for most of the range of ν_r that is examined. If we extrapolate this behavior to the LPE data shown in Fig. 11, it is reasonable to attribute the drop in $LW_n(obs)$ between $\nu_r = 1$ and 2 kHz to a MAS averaging of some of the $J(n\omega_r)$ terms.

Equation [10] also becomes a means for testing whether the experimental *magnitude* of $LW_n(ORPI)$ can be reproduced, assuming $\tau_s = 33$ μs for the Lorentzian spectral density and $\tau_s = 28$ μs for the exponential spectral density. Recall that these τ_s's gave the best fit to the ν_r dependence of the parabolic coefficients, even though the magnitudes of $LW_f(ORPI)$ calculated were 10–20% below those observed. Substitution of these τ_s's into Eq. [10] predicts a $LW_n(ORPI)$ for the Lorentzian spectral density which is only 35% of that observed; for the exponential spectral density, the predictions are 47% of observed. This agreement is significantly worse than that for $LW_f(ORPI)$. Therefore, we also adapted the previously described Monte Carlo calculations so that we could predict on-resonance linewidths. We first duplicated the results of Eq. [10] for independently fluctuating proton spins with a single lifetime of twice the correlation time in Eq. [10]. Then, we calculated $T_{2n}^C(ORPI)^{-1}$ for the two-lifetime model previously described. The lifetime parameters, $\tau_{sh} = 80$ ms and $\tau_{lg} = 160$ μs, which fit reasonably well the shape of the ν_r versus b data (Fig. 12), yielded $LW_n(ORPI)$ values about 10% below experimental. This is good agreement in view of a 10–15% increase expected if contributions from more distant protons are included in the calculation. (It turns out that in the two-lifetime model for OR-LPE, it is the states with $I_z = \pm 1$ that contribute most heavily to dephasing for the on-resonance case; hence, for OR-LPE, one has the situation that the lifetime for the $I_z = 0$ state is dominant in determining the off-resonance behavior and the lifetimes in the $I_z = \pm 1$ states are dominant in determining the on-resonance behavior.)

While we may take satisfaction that the two-lifetime model gave better agreement with both the $LW_f(ORPI)$ and the $LW_n(ORPI)$ data for OR-LPE, the principal reason for the failure of the single-lifetime spectral densities is that they are not sufficiently "peaked" at $J(0)$. A τ_{lg} of 160 μs served to produce the proper "peaking." Recall, however, that the two-lifetime model utilizes Lorentzian spin correlation functions which do *not* conceptually include the long tails associated with the idea of conservation of total polarization. Proper

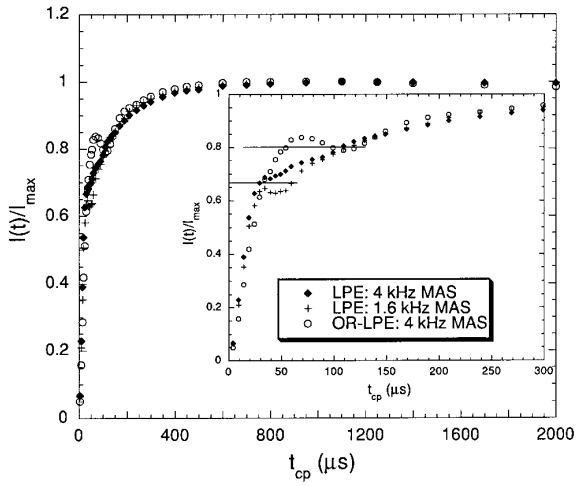

FIG. 13. Normalized cross-polarization amplitudes at 2.35 T for the polyethylene samples given in the legend as a function of cross-polarization time under optimized matching conditions where $\nu_1^H = 65$ kHz $= \nu_1^C - \nu_r$. The inset expands the early-time behavior. A qualitative argument given in the text relates the time ($\approx$80 μs) required for going from an amplitude of 0.67 to 0.80 to one-half the characteristic time for polarization exchange between a $^{13}CH_2$ proton and a more distant proton.

inclusion of this effect might also, in principle, supply the needed amplitude at $J(0)$ for giving agreement with LW_n(ORPI). Another reason to be skeptical about the two-lifetime model is the following. It is not compellingly obvious that for the *i*th proton, spin flips with its single intramethylene proton partner at a distance of 0.178 nm should dominate the *summed* influence of the other 15 protons that lie within 0.31 nm, given that r_{ij}^{-3} for the intramethylene pair in LPE is less than 20% of $\Sigma_j\, r_{ij}^{-3}$ for that *i*th proton. We now turn to some cross-polarization (CP) data which offer qualitative commentary on the validity of the two-lifetime model.

A rough estimate of τ_{lg} may be obtained from the 2.35 T, CP data for LPE and OR-LPE in Fig. 13. The inset provides an expansion of the data at earlier times. The horizontal lines are drawn there at amplitudes of 0.67 and 0.80. These lines correspond to ^{13}C polarization levels expected when full equilibration is reached for three spins (one ^{13}C and two bonded protons) and five spins (one ^{13}C plus two bonded and two non-bonded protons), respectively. We expect the required increment of time for covering the interval from 0.67 to 0.80 to be slightly longer than $\tau_{lg}/2$. The foregoing expectation is based on ^{13}C polarization exchange only with its bonded protons during cross-polarization. (A consideration of direct polarization exchange between ^{13}C nuclei and more distant protons would cause us to *underestimate* τ_{lg} when applying the foregoing claim.) In Fig. 13, there is a break in the LPE curves near 0.67 indicating that the fastest process is intramethylene spin equilibration (*36*); this process is complete in only about 30 μs. Then a longer process takes over whose detailed shape is dependent on ν_r but whose overall rate of change at longer times is similar for the three data sets shown. The 0.80 polarization level is reached at $t_{cp} \approx 110$ μs in all of the samples, ignoring the oscillation of the OR-LPE data; in other words, the five-spin equilibrium level is reached about 80 μs after the three-spin level is reached. Very crudely then, this 80 μs difference would be identified with a time slightly longer than $\tau_{lg}/2$, implying a τ_{lg} of $\approx$140 μs, i.e., comparable to the τ_{lg} of 160 μs in the model calculation. This is further support for the notion that spin exchange between a proton inside and a proton outside of the $^{13}CH_2$ group is significantly slower than that between protons within this group.

We now summarize this exercise of trying to extract information about the spectral density function associated with spin fluctuations. Our main objective is to specify some critical timescales for decoupling strategies, such as TPPM, that attempt to reduce LW(ORPI) contributions. These strategies introduce secondary fields whose purpose is to promote "second averaging" of $\langle I_{zi}\rangle$. An important issue is to define the *shortest* time scale for the fluctuations; this is the time scale over which one would want significant "second averaging." From the fits to the data shown in Fig. 12, we would suggest that a τ_s of 25 μs, corresponding to a 50 μs spin lifetime, would be a conservative estimate of the shortest τ_s over any orbit. Also, the spectral density function definitely exhibits a "peaked" behavior at $J(0)$. The practical importance of this peaking is that the threshold for good second averaging in TPPM will be more diffuse than it would be for, say, a Lorentzian spectral density function. In other words, application of what might seem to be inadequate rates of second averaging may still produce some improvement in resolution.

Brief Comments Regarding MAS-Assisted Dipolar Fluctuations (MADF)

While the focus of this paper is the influence of ORPI on linewidths, the strong broadening from the mechanism we refer to as MADF merits a brief, albeit more qualitative discussion. We can point to at least two features associated with MADF broadening which seem to necessitate a mechanism distinct from that used to explain the ORPI line broadening. First, from Fig. 7, the onset of this broadening is quite abrupt and becomes quickly dominating. Particularly at lower B_0 where the influence on LW_n(ORPI) from proton CSA is negligible, this rapid onset remains. Second, in the theory used to understand ORPI line broadening, there is no reason why, for a given ν_1^H, linewidths should *increase* as ν_r increases, as is seen in Fig. 11.

In an earlier paper (*4*), before the dependence of MADF broadening on ν_r was appreciated, this mechanism was called "insufficient decoupling power" and was explained in terms of cross-polarization with an RF mismatch of ν_1^H in the limit where $\nu_1^C \rightarrow 0$. Again, a simple picture of the influence of MADF starts out with the notion that sizable perturbations between *I* and *S* spins in rigid lattice systems can be understood by projecting all relevant spin motions along the static field direction (the *z*-axis). For explaining LW(ORPI) one draws

attention to the small z-projections, $\langle I_{zi}\rangle$, of the proton spin components, $I_{z'i}$, which are *parallel* to $\nu_{\text{eff}}^{\text{H}}$; in contrast, in order to explain MADF broadening, one considers the usually larger z-projections, $\langle I_{zi}\rangle_{\text{m}}$, of the $I_{x'i}$ components, which are transverse to $\nu_{\text{eff}}^{\text{H}}$. The subscript "m" refers to "modulation" because the $I_{x'i}$ components are modulated, i.e., precess, at the nominal frequency of ν_1^{H} in the presence of the proton RF field.

In the *absence of MAS*, the idea used (*4*) to explain the broadening from insufficient decoupling power is that dipolar fluctuations, arising from mutual spin-flips between proton pairs, frequency-modulate (*37*) the precession of $I_{x'i}$ (and of $\langle I_{zi}\rangle_{\text{m}}$); thus, the resulting time dependence of $\langle I_{zi}\rangle_{\text{m}}$ is expressed in terms of an associated correlation function having a distribution of spectral densities centered around ν_1^{H}. In the presence of sufficiently fast spin-flip modulations, this spectral density can take on some zero-frequency character. Such zero-frequency spectral density causes a T_2^{C}-type dephasing in a non-spinning sample via the heteronuclear Hamiltonian (Eqs. [1] and [4]). If ν_1^{H} is large enough, this spin-flip-induced modulation of the spin precession will not yield any significant spectral density at zero frequency since the highest frequencies of spin-flip modulation lie below ν_1^{H}. As ν_1^{H} decreases below a threshold value of ν_1^{H}, which is about 40 kHz for LPE, this spectral density *at zero frequency* will become non-negligible and rapidly increase.

If MAS is now added to the foregoing picture, then, in Eq. [4], $\omega_{\text{D}i}$ becomes fully amplitude-modulated (*37*) by conversion into the sum of terms having periodicities of ω_{r} and $2\omega_{\text{r}}$ (see Eq. [6]). Thus, the spectral density, $J_{\text{lf}}(\omega)$, associated with the time dependence of the local proton fields, $\omega_{\text{D}i}\langle I_{zi}\rangle_{\text{m}}$, includes the coherent time dependence of $\omega_{\text{D}i}$ and the coherent-plus-incoherent time dependence of $\langle I_{zi}\rangle_{\text{m}}$. It is easy to see how the range of the spectral density associated with $\langle I_{zi}\rangle_{\text{m}}$ alone is narrower in frequency than $J_{\text{lf}}(\omega)$ since the latter includes the time dependence of $\omega_{\text{D}i}$. Thus, within the range of ν_{r} where the rate of proton spin-flips is unaffected by faster spinning, it is easy to rationalize that faster spinning increases the total width of $J_{\text{lf}}(\omega)$ for LPE, thereby increasing both $J_{\text{lf}}(0)$ and the threshold value of ν_1^{H} at which LW(MADF) becomes significant.

Two published papers, both dealing with adamantane, are relevant to this discussion of MADF broadening. Stejskal *et al.* (*37*) discuss the influence of dipolar fluctuations in combination with MAS on the heteronuclear dipolar Hamiltonian. The context is a description of cross-polarization. The amplitude modulation, via MAS, of $\omega_{\text{D}i}$ and the frequency modulations, via dipolar fluctuations, of $I_{x'i}$, are shown to result in a multiply peaked plot of cross-polarization rate against RF amplitude when the other RF amplitude is held fixed. In such a plot, it is shown and rationalized that one should see maxima, separated by ν_{r}, on both sides of the condition $\nu_1^{\text{H}} = \nu_1^{\text{C}}$ and that the first two maxima dominate even though higher order maxima also exist. The second relevant paper (*29*) describes a deterioration of resolution in adamantane whenever the condition $\nu_1^{\text{H}} = n\nu_{\text{r}}$ is met. This result was described in terms of "rotational resonance recoupling" of the ^{13}C–^{1}H dipolar interaction. This picture describes MADF broadening for the special case where the width of the frequency modulation associated with spin flips is smaller than ν_{r}. For the ν_{r} range that we have explored, LPE is in the contrasting regime where spinning seems to have little influence on the width of these fluctuations.

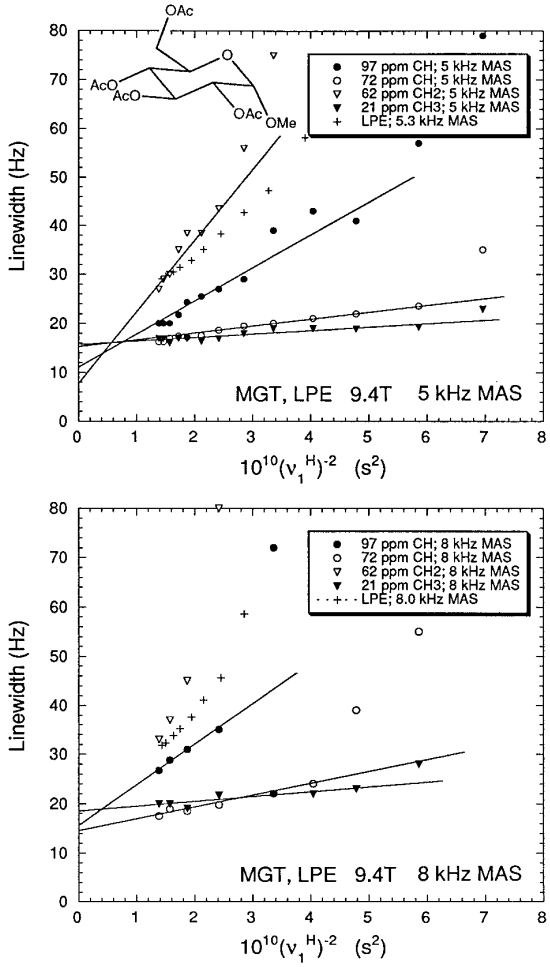

FIG. 14. On-resonance linewidths at 9.4 T for $\nu_{\text{r}} = 5$ kHz (upper) and $\nu_{\text{r}} = 8$ kHz (lower) plotted against the inverse square of the RF field for selected carbons of MGT whose structure is shown. Corresponding data for LPE are added for comparison. The various kinds of carbons are indicated in the legends. Note the insensitivity of the methyl linewidths and the significant variation in sensitivity for the methine carbons.

On the Generalizability of These Results to Other Protonated Carbons

We performed a few linewidth measurements at 9.4 T on methyl-α-D-glucopyranoside tetraacetate (MGT). The molecule making up this crystalline material possesses a variety of carbons with the full range of bonded protons. Figure 14 shows the molecular skeleton of MGT along with observed linewidths for selected methyl, methylene, and methine carbons as a function of $(\nu_1^{\text{H}})^{-2}$; the upper and lower data correspond to ν_{r}

TABLE 3

Parabolic Coefficients for One Methylene and Two Methine Carbons in MGT at 9.4 T, $\nu_1^H = 73$ kHz, and the Two Indicated Values of ν_r

Resonance (ppm)	Carbon type	b ($\times 10^{-6}$ s) at 2 kHz	b ($\times 10^{-6}$ s) at 5 kHz
62	CH_2	17.9 ± 0.5	8.8 ± 0.5
72	CH	4.2 ± 0.2	1.2 ± 0.1
97	CH	3.2 ± 0.2	1.0 ± 0.1

Note. Errors represent one standard deviation in the parabolic fitting procedure.

values of 5 and 8 kHz, respectively. Also shown, for comparison, are the corresponding LPE data. Not shown are our LW(obs) versus $\Delta\nu_{RF}$ data which indicated that the mean proton resonance for all of the methine and methylene protons is within ±300 Hz of the frequency used to obtain the data of Fig. 14; Table 3 gives the corresponding parabolic constants, *b*, obtained from the latter data. The data of Figure 14 may thus be considered to represent "on-resonance" linewidths, given that the maximum linewidth contribution from off-resonance effects in Fig. 14 would be 0.2 Hz for the methine carbon and 0.5 Hz for the methylene carbon. The data are somewhat noisy, reflecting the limited time available on the 9.4 T instrument. It was not our goal to broaden the scope of this study; yet we wanted a little perspective on how generalizable the polyethylene results were; the experiments at 9.4 T would show this most clearly.

A very notable characteristic of the MGT lineshapes, which became more evident at lower ν_1^H's and larger $\Delta\nu_{off}$'s, was the development of lineshapes which looked like a narrower resonance sitting atop a broader base, as though there might be some "inhomogeneous" broadening present. These lineshapes stand in contrast to the LPE lineshapes which, while sometimes asymmetric, always had more smoothly changing contours. Figure 15 shows the non-acetyl portion of two "on-resonance" spectra of MGT at $\nu_r = 5$ kHz and ν_1^H values of 68.7 (top) and 41.3 (bottom) kHz. Assignments are indicated in the caption. The lower spectrum illustrates more clearly the narrower and broader features of certain lineshapes, notably those at 97 and 62 ppm. The linewidths shown in Fig. 14 are based on FWHH measurements. In the presence of such lineshapes, the FWHH measurement demands that a peak amplitude be selected. We did this somewhat subjectively, considering the signal-to-noise ratio, with the result that, for these more cusp-like lineshapes, we invariably chose a peak height about 1 rms noise level below the observed peak height. Needless to say, these lines are generally not Lorentzian. We did not do T_2^C measurements, which would have helped to sort out the inhomogeneous character of the line.

With the foregoing considerations in mind, from Fig. 14 and Table 3 we conclude the following: (a) The single methylene carbon at 62 ppm shows a significantly steeper slope (≈1.8×) at 5 kHz than LPE. (b) The methyl carbon at 21 ppm shows very little sensitivity to ν_1^H; hence, LW_n(ORPI)'s are small for these methyl carbons. (c) The methine carbons show a dependence on ν_1^H which is intermediate between the dependences of the methylene and methyl carbons; yet, the contrast in behaviors of the two methine carbons is quite large, i.e., the 97-ppm methine carbon (attached to the methoxy group) has much larger (×3 to ×4) contributions from LW_n(ORPI) than does the unassigned, 72-ppm methine carbon. That these differences in methine behaviors can be traced to proton CSA effects is further supported by intensity-related observations, mentioned in the caption of Fig. 15, pertaining to 4.7 T MGT spectra. (d) Both the methylene and the methine carbons show departures from a linear dependence on $(\nu_1^H)^{-2}$ as ν_1^H decreases. Considering the previously mentioned reason for this departure (MAS-assisted dipolar fluctuations near ν_1^H) and considering how the threshold for observing this mechanism depends on ν_r

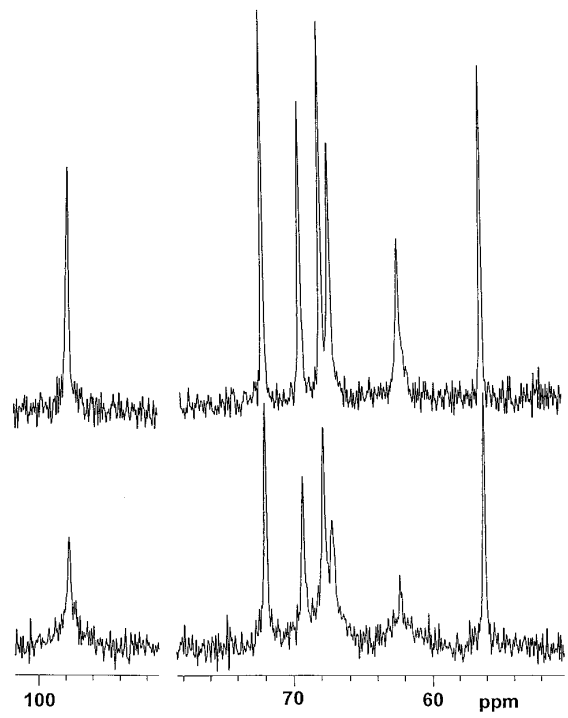

FIG. 15. On-resonance spectra at 9.4 T for the non-acetyl resonances of MGT at $\nu_r = 5$ kHz and $\nu_1^H = 69$ kHz (upper) and 41 kHz (lower). All resonances are methine resonances except at 62 ppm (methylene) and 56 ppm (methyl of the methoxy group). Note the substantial variation in linewidths for the methine carbons and the heterogeneous appearance (a narrower line astride a broader base) of the 98 and 62 ppm resonances at $\nu_1^H = 41$ kHz. The variation in peak heights over the different methine groups as well as the methylene group is strongly accentuated at higher static fields as expected when proton CSA interactions dominate the ORPI contributions to linewidth. For example, for an MGT spectrum (not shown) taken at 4.7 T with a choice of parameters comparable to the upper spectrum, peak height ratios for the 97 (CH) and 62 (CH_2) ppm peaks, relative to the 72 (CH) ppm peak height, are, respectively, 0.89 and 0.73; in the upper spectrum at 9.4 T these same ratios are 0.61 and 0.40.

(Fig. 10), it is no surprise that this point of departure in Fig. 15 is similarly dependent on ν_r. In addition, this point occurs at a lower value of ν_1^H for a methine carbon than for the methylene carbon. The latter observation implies that the spectral density of fluctuations extends to higher frequencies for a methylene than for a methine carbon as would be expected for methylene carbons whose protons can undergo spin flips with each other. (e) The relative similarity of the *b* values in Table 3 for the two methine carbons suggests that the rates of spin fluctuations at these two sites are only modestly different. Therefore, the explanation for the different slopes these carbons exhibit in Fig. 14 must mostly reflect a contrast in the proton CSAs; either the magnitudes are different by about a factor of two or the tensor orientations, relative to the corresponding ^{13}C–H internuclear vectors are different. The relative orientation of the two tensors determines the magnitude of the $J(0)$ coefficient in the $T_{2n}^C(\mathrm{ORPI})^{-1}$ expression. (If one knew more about the details of the proton CSAs in various bonding situations, one could conceivably use a plot like Fig. 14 as a carbon assignment tool.) (f) The *b* values for the methylene carbon in MGT are about 30% higher at $\nu_r = 2$ kHz and about 65% higher at 5 kHz than those for the carbon in LPE. Application of Eq. [7], using the isotropically averaged coefficients for Lorentzian spectral densities, gives a τ_s of 34 μs, based solely on the ratio of the *b*'s at the different ν_r. At the same time, this τ_s predicts magnitudes for the *b*'s which are $\approx$75% of those observed. It is not an intuitive result that τ_s should be 34 μs in MGT and 47 μs in LPE, considering the higher proton density in LPE unless the greater isolation of the $^{13}CH_2$ group fosters more rapid spin flips between these protons. We reserve judgment on this issue and await more careful experiments with better signal-to-noise.

In summary, the MGT data, in spite of the marginal signal-to-noise, have indicated that methyl carbons are not strongly influenced by $LW_n(\mathrm{ORPI})$, methine carbons have quite variable, but intermediate contributions from $LW_n(\mathrm{ORPI})$, and methylene carbons can have even greater contributions to $LW_n(\mathrm{ORPI})$ than the carbons in LPE. In addition, the narrow/broad aspects of some of these lineshapes deserve further scrutiny. Is this the result of fewer distant non-^{13}C-bonded protons? In LPE, of the 15 neighboring protons that lie between 0.247 and 0.310 nm from each methylene proton, 8 of these are intramolecular pairs; for the methylene protons of MGT, the maximum number of such intramolecular pairs is 2 and, it may be less, depending on the stereochemical disposition of the methylene group. Thus, these methylene protons in MGT are clearly more isolated, in a polarization-exchange sense, from neighboring protons, relative to the protons of LPE. Another qualitative argument for widely disperse linewidths is the recognition that when ^{13}C–H internuclear vectors are parallel to the spinner axis, ($\beta_i = 0$), then $\omega_{Di} = 0$ at every point in the orbit; hence, there is no contribution to LW(ORPI) from that proton. $LW_n(\mathrm{ORPI})$ contributions would then arise from other protons with non-zero β_i's. For a methylene carbon such contributions would mainly originate from the other attached proton. For methine carbons, LW(ORPI) would be relatively small, arising from more distant, weakly coupled protons. If this were the principal argument, we would expect the dispersion in methine linewidths to be more evident than that for the methylene resonance. Contrary to such an expected trend, narrow-linewidth components, in Fig. 15, are seen for both methylene and methine carbons.

There should also be a probing into the question of whether broadening in MGT is entirely a T_2^C broadening, as in LPE, or whether some proton spin states are so long lived that the effects on the carbon resonance must be partially described in static-spin-state terms (*2*). Evidence already exists for nonspinning organic single crystals that certain, more isolated protons, have very long spin-state lifetimes at certain orientations (*9*). Admittedly the latter observation was made for a methine proton at an orientation where the ^{13}C–H dipolar interaction was near maximum and ν_1^H was relatively weak. Thus, the presence of the ^{13}C dipolar interaction contributed significantly to the "isolation" of the attached proton from the rest of the protons; this attached proton would be much less isolated at higher ν_1^H. Also, structure-related isolation of protons from spin–exchange interactions would be an important issue to elucidate, not only for considerations of resolution but also for understanding cross-polarization dynamics and the quantitative character of cross-polarized signals. In the context of improving resolution, however, by implementation of strategies like TPPM (*1*), the issue of spin–exchange isolation becomes somewhat less important in that a properly conceived and implemented TPPM decoupling should be effective in reducing LW(ORPI) contributions, regardless of whether the origin is a T_2^C contribution or a static linebroadening (*1, 2*). In fact, spin isolation will usually relax the criteria for second averaging in a scheme like TPPM since MAS averaging, acting in parallel with TPPM averaging, would also be very efficient. This leads us to comment further on new decoupling schemes, like TPPM.

Relation of This Work to the Choice of Parameters for CW Decoupling and Some Perspectives on New Decoupling Schemes

New decoupling methods, like TPPM, incorporate the idea of generating, via some modulation strategy, a second, weaker RF field, ν_2^H, orthogonal to both the static field and the main RF field. This second field is designed to average away these residual proton spin projections along the static field direction (Eq. [1]). In this way the LW(ORPI) contributions will be reduced, provided that the precession period, $(\nu_2^H)^{-1}$, corresponding to this second field is significantly shorter than the minimum effective proton spin-state lifetimes. If we take 50 μs to be an approximate minimum spin lifetime in LPE, as discussed, then the condition $\omega_2^H\tau_{\mathrm{eff}} = 1$ is obtained when $\nu_2^H =$ 3.2 kHz. This field strength is a threshold value for influencing

resolution. One would anticipate that ν_2^H ought to be at least 5–10 kHz in order to be reasonably effective in reducing the resident spin fluctuations. In other words, we expect the minimum effective ν_2^H to be slightly higher than that ν_r ($\approx$5 kHz) which gives a significant attenuation for the *b* values (Fig. 6). We say "slightly higher" since ν_2^H produces modulations of I_{zi} only at ν_2^H, whereas ν_r produces modulations at both ν_r and $2\nu_r$. However, one cannot arbitrarily choose ν_r and ν_2^H since both are coherent frequencies imposed on the system. As has been discussed before (*1*), one of the constraints on the modulation schemes is that one wishes to avoid interference between ν_r and ν_2^H; usually this means avoiding the conditions where $m\nu_r = \nu_2^H$ or $\nu_r = n\nu_2^H$ with *m*, *n* integers. The condition, $\nu_2^H > \nu_r$, seems slightly more desirable than $\nu_2^H < \nu_r$, for averaging ORPI contributions since the modulation of I_{zi} via ν_2^H acts on a wider range of LW(ORPI) contributions than does ν_r.

A central point is that *it is mainly the LW(ORPI) contribution, including both LW_f(ORPI) and LW_n(ORPI), which is susceptible to improvement via TPPM.* Other, mostly inhomogeneous, contributions to linewidth, e.g., anisotropic bulk magnetic susceptibility (*4*), can be much larger than LW_n(ORPI); TPPM will do nothing for such contributions. LW_n(ORPI) contributions can be estimated, from plots like Figs. 8 and 14, as the difference between the actual linewidths and the intercept values at infinite power. (Note that in the regime where molecular motions have characteristic frequencies less than ν_1^H, these motions can also give (*4*) a dependence of linewidth on $(\nu_1^H)^{-2}$. Such contributions to linewidth will increase the slopes of plots like those in Figs. 8 and 14. Considering the nature of this motional relaxation mechanism, TPPM is not expected to be particularly effective in removing this broadening. Therefore, when significant relaxation due to slow motion is present, plots like Figs. 8 and 14, taken at a single B_0, will only give upper limits for LW(ORPI).

An important perspective in estimating the benefits of TPPM is that the LPE and MGT cases represent systems in which two important situations prevail: First, broadening from molecular motion is negligible and broadening from anisotropic bulk magnetic susceptibility is about as small as it is for any organic system; therefore, *the relative contribution from LW_n(ORPI), as a fraction of the total linewidth, is larger than in similarly composed materials which display motional or susceptibility broadening.* Second, LPE and MGT are *NOT representative of those materials which have other major sources of local fields which, in turn, can give rise to greater LW_n(ORPI) effects.* In particular, very localized dipolar fields from, say, nitrogen, phosphorus, chlorine, or fluorine nuclei can create varied and possibly large LW_n(ORPI) contributions when ^{13}C nuclei are coupled to protons in close proximity to these other types of nuclei. Therefore, especially at lower B_0, measurement of LW_n(ORPI) might be used to assign ^{13}C resonances in the vicinity of third magnetic nuclei. Correlations of linewidths and T_2^C's with distance to ^{19}F nuclei in lightly fluorinated solids have already been observed (*38*), and there is a reasonable chance that LW_n(ORPI) will also show dependence on the relative orientations of the ^{13}C–H and the ^{19}F–H dipolar tensors.

These dipolar local fields fall into a category for broadening similar to the CSA of the protons (except for the B_0 dependence of the CSA), since these fields are second-rank tensors. Expressions like Eq. [10] involving $J(0)$ are expected. Thus, in the paper in which TPPM was introduced (*1*), the presence of ^{15}N in the materials described significantly enhanced the relative contributions of LW(ORPI). Therefore, TPPM yielded a greater improvement in linewidth than would have been seen in the absence of the ^{15}N nuclei. Also, *the MGT and LPE results are not representative of samples like soil samples, where there can be macroscopic inclusions of high magnetic susceptibility.* It has already been shown (*10, 11*) that slow modulation schemes for decoupling can improve resolution (mainly demonstrated effective for carbons with weak proton couplings) in such soil samples. Again, robust TPPM sequences should greatly improve these linewidths, with the degree of improvement depending somewhat on whether the inclusions have isotropic or anisotropic bulk susceptibility.

In our treatment of LW_n(ORPI) in Eq. [10], we considered the proton CSA to take on its experimentally determined value. From Table 1, however, it is clear that we should be dealing with an effective CSA which includes susceptibility effects. This brings up a point which will usually be a minor effect, but could become significant at higher B_0, namely that there is a mechanism here where particle shape and the intra- and interparticle susceptibility fields may increase the size of the "effective CSA," hence the amount of broadening. MAS averages to zero the local field perturbations, arising from isotropic bulk magnetic susceptibility, at the ^{13}C nuclei; however, a *shortening* of T_2^C could also very well be traced to the corresponding susceptibility fields sensed by the protons. Therefore, at high fields one may see some improvement in resolution when going from a polycrystalline sample to a monolithic, void-free solid sample with ellipsoidal shape (although the presence of the rotor endcaps and their susceptibility effects must also be considered). For LPE in these studies, we used solid plugs, snugly set against endcaps.

Our data indicate that, in comparison to the ORPI mechanism, the potential of MAS-assisted dipolar fluctuations (MADF) for dominating linewidths is much greater. While TPPM strategies can reduce contributions from LW_n(ORPI), it is doubtful whether similar benefits are available from TPPM for linewidth contributions from MADF. This point should be verified experimentally. Our skepticism about the efficacy of TPPM for reducing line broadening associated with MADF in a material such as LPE is that the most important ingredient for generating undesirable "zero-frequency spectral density," $J_{lf}(0)$, associated with the proton local field, is spin-flip modulations. Since the width of these modulations in the presence of CW decoupling extends to about 40 kHz, we do not see how

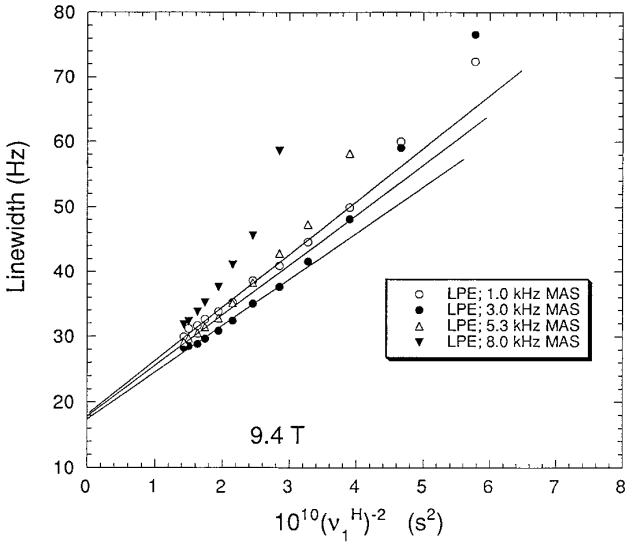

FIG. 16. Plots, like those if Fig. 8, for LPE at 9.4 T at the various ν_r given in the legend. Note that at $\nu_r = 8$ kHz one can no longer identify a final slope. This suggests that for $\nu_r = 8$ kHz, MADF contributions are no longer negligible, even at $\nu_1^H = 80$ kHz.

the slower rates of second-averaging in the TPPM sequence will significantly slow these fluctuations. In fact, TPPM may cause additional MADF broadening, relative to CW decoupling at the same ν_1^H, by imposing additional coherent time dependences on $\langle I_{zi}\rangle_m$. There is, therefore, an associated possibility that $J_{lf}(\omega)$, whose spectral density distribution is centered at ω_1^H, might become broader in the presence of TPPM with the result that $J_{lf}(0)$ and the ^{13}C linewidth could increase. A primary practical concern, therefore, is to have a sufficiently large ν_1^H available so that this broadening mechanism is not important.

In order to emphasize the influence of MADF, we replot in Fig. 16 some of the LPE linewidth data from Fig. 10b against $(\nu_1^H)^{-2}$ for various values of ν_r. From Fig. 16, it is apparent that the region of linear dependence on $(\nu_1^H)^{-2}$ shrinks quite rapidly as ν_r increases. For $\nu_r = 8$ kHz, there is no well-defined linear region. In other words, the contributions from MADF are becoming perceptible at $\nu_r = 8$ kHz even when ν_1^H lies in the range 80–90 kHz.

In terms of our qualitative understanding of MADF broadening, the data of Fig. 10a make more sense than the data of Fig. 10b. In the data of Fig. 10a, we see that ν_r augments the dipolar fluctuations by about $2\nu_r$ at 2.35 T, consistent with other observations (*29*) and the notion that modulation, by MAS, of ω_{Di} at ν_1^H and $2\nu_1^H$ is a dominant contribution to the broadening of $J_{lf}(\omega)$. On the other hand, augmentation by about $3\nu_r$ above $\nu_r = 4$ kHz at 9.4 T (Fig. 10b) is not so easily understood unless, for example, further modulations associated with the proton CSA are possible. (There is a chance that this 9.4 T data is reflecting the greater RF instability of this spectrometer relative to the spectrometer at 2.35 T; on the other hand, the OR-LPE data at 9.4 T showed the very same trend.) Nevertheless, smaller effects at $3\nu_r$ and even $4\nu_r$ are certainly present (*29*); so evidence for measurable MADF contributions at higher ν_1^H in plots like Fig. 16 for $\nu_r = 8$ kHz is not surprising.

Finally, we offer some general remarks on parameter selection for the optimization of resolution, keeping in mind the perceived trend toward operation at higher static fields and larger ν_r. For CW decoupling, it is very clear that for rigid methylene and methine carbons, in the absence of third magnetic nuclei or problems with large internal susceptibility fields, the preservation of resolution demands that ν_1^H increase significantly as B_0 increases. For LPE or MGT, 55 kHz is more than adequate at 1.4 T, 60 kHz is reasonable at 2.35 T for ν_r up to 4 kHz, and 70 kHz seems adequate at 4.7 T (at least up to $\nu_r = 5$ kHz, but not necessarily up to 8 kHz). However, it seems apparent that one ought to have at least 90–120 kHz available at 9.4 T, depending on the ν_r chosen. These values of ν_1^H are based to some extent on the fact that LW_n(ORPI) (expressed in Hz) has a B_0^2 dependence (Eq. [10]) at constant ν_1^H. Of greater concern, however, is the importance of the broadening from MADF. As previously mentioned, according to Fig. 10b, the ν_1^H at which one sees a strong onset of broadening at 9.4 T increases at about three times the rate of increase of ν_r. Also from Figs. 10b and 16, it would seem desirable to have a ν_1^H of 80–90 kHz at $\nu_r = 8$ kHz. If one were further tempted to avoid sideband/centerband overlap in a general CPMAS spectrum at 9.4 T by using $\nu_r \approx 16$ kHz, then if the trends of Fig. 10b continue, one would want a corresponding ν_1^H of about 105–115 kHz. Whether the trend noted in Fig. 10b continues depends in part on whether the basic rate of spin fluctuations, which MAS modulates, is independent of ν_r. As ν_r increases, there will come a point where the rate of these fluctuations will decrease. The ν_r at which this happens may be a sensitive function of the local proton distribution. We will not speculate on how fast one must spin to achieve this. The relative flatness of the LPE LW(obs) versus ν_r curve at 9.4 T in Fig. 11b for $\nu_1^H = 83.6$ kHz suggests that the rate of spin flips is quite constant (i.e., $J(0)$ is quite constant) in LPE up to $\nu_r = 8$ kHz. We do not claim any similar observation in MGT.

In the limit of very fast MAS, long spin lifetimes are expected. The "on-resonance" ORPI contributions to linewidth will then be heterogeneous (*2*) and will be larger than they would have been had spin fluctuations been present. Therefore, if no TPPM-like strategies are applied, and if ν_1^H is large enough that MADF give negligible contributions to the linewidth, then MAS-induced quenching of spin fluctuations will degrade resolution.

The blessing/curse aspect of fast MAS is important for the experimentalist to recognize. There are the negative issues, namely, the non-trivial complications for reliable cross-polarization (*39*) along with the points just discussed, i.e., the need for higher ν_1^H's and the potential that LW_n(ORPI) effects will increase. On the other hand, fast MAS offers the advantages of

fewer spinning sidebands (simpler spectra and better signal-to-noise in the centerbands), and a reduced sensitivity to $\Delta\nu_{RF}$ (see Fig. 6). The latter benefit is significant, given that one typically chooses a mean decoupler frequency in the presence of a dispersion of proton chemical shifts. At the same time, Fig. 6 also suggests that changes in the parabolic coefficient are small beyond $\nu_r \approx 6$ kHz even though Eqs. [7], [8a], and [8b] do not predict a flatness at higher ν_r. Fast MAS also has significant advantages in reducing homonuclear coupling effects in the CPMAS spectra of fully-^{13}C-labeled materials (*40*).

We now make some comments about *lineshape.* The OR-LPE data have allowed us to retain some simplicity in our analysis in terms of spin fluctuations. These data, together with the data from the unoriented sample, have also experimentally verified a dependence of LW(ORPI) on crystalline orientation within the rotor. Therefore, *the notion that CPMAS lineshapes in a polycrystalline sample ought to be Lorentzian, for the purposes of lineshape fitting, should be regarded as theoretically unjustified.* Experimentally, we encountered only a few regions of parameter space where lineshapes were closely Lorentzian for either sample. For the most part, lineshapes had a little asymmetry and had wings which were either too intense or too weak compared with the wings of corresponding best-fit Lorentzian lines. Distributions of T_2^C(ORPI) values, to the degree that they dominate the lineshape, should give rise to symmetric, not asymmetric, lineshapes with wings somewhat more intense than those of the best-fit Lorentzians. However, second-order dipolar shifts, distributions of Bloch–Siegert shifts, the detailed shape of the B_0 field across the sample, and chemical shift dispersions intrinsic to the sample may all contribute to lineshape asymmetry. With strong decoupling close to resonance, the lineshapes at 2.35 T had wings which fell off in intensity faster than those of the optimized Lorentzian fits. At higher fields, the experimental wing intensity varied both above and below that for the optimized Lorentzian fits; moreover, the asymmetry became more evident.

We digress to one other observation on the subject of non-Lorentzian lines. It seems reasonable that full plots, like one shown in Fig. 3, should identify the isotropic-average proton resonance frequency with the center frequency of the parabola; we adopted this definition. Recall, however, that when we changed samples from the unoriented to the oriented LPE samples, we saw a shift in this central frequency, as though the field inside the sample had *both* remained the same for the ^{13}C nuclei and had increased by about 0.6 ppm for the protons. Such an interpretation is absurd. The qualitative explanation for this relative shift is that the parabolic minimum occurs when the orbit-averaged T_2^C values are *collectively* maximized over all orbits represented. Orbit-averaged T_2^C(ORPI) values are, to the degree that we can ignore the orientation dependences of the spectral density, a time-weighted average of $(\omega_{Di}\Delta\omega_{off}(i))^2$, i.e., of the *squares* of the instantaneous deviations from ^{13}C resonance (Eq. [3]) experienced over the orbit. On-resonance, we presume that $\Delta\omega_{off}(i)$ is dominated by the proton CSA (Eq. [9]); thus, $\Delta\omega_{off}(i) = \Delta\omega_{CSA}(i) + \delta_i$, where δ_i is the difference between the true resonance frequency for the ith proton and its apparent resonance frequency, $2\pi\nu^*_{RF}$, defined by the parabolic minimum of the ^{13}C resonance (Fig. 3). Within the approximation that for LPE, the ^{13}C–H dipolar tensor and the proton CSA tensor are collinear and axially symmetric, the existence of and the sign of the difference in ν^*_{RF} values for OR-LPE and LPE can be understood quite simply. Critical to the argument is the recognition that, for the two $^{13}CH_2$ protons *over any MAS orbit,* the $(1 - 3\cos^2\theta_i)$ angular dependence of $\Delta\omega_{CSA}(i)$ and ω_{Di} is not only the same but almost always *asymmetric* with respect to positive and negative deviations from the mean. Moreover, when asymmetric, the maximum deviation of $(1 - 3\cos^2\theta_i)$ is always larger in the negative direction. Only for $\beta_i = \pi/2$ (the OR-LPE case) and for $\beta_i = 0$ (a condition that cannot simultaneously be true for both methylene protons) are the positive and negative excursions from the mean symmetric (for $\beta_i = 0$, there are no excursions). It is easy to prove that when excursions are symmetric, i.e., $\beta_i = \pi/2$, the orbit average of $(\omega_{Di}\Delta\omega_{off}(i))^2$ (a quantity proportional to the instantaneous LW(ORPI) at a particular orientation) is minimized when $\delta_i = 0$; so, for OR-LPE, ν^*_{RF} represents true resonance. For all other orbits, which have asymmetric excursions, it can be easily demonstrated that δ_i becomes non-zero and orbit-dependent; however, *the sign of* δ_i *is always the same* such that ν^*_{RF} moves away from the true mean resonance and in the direction of that proton resonance associated with the unique axis of the proton CSA tensor. Thus, for LPE where ν^*_{RF} lies upfield from its OR-LPE counterpart, we infer that within the approximation of the collinear, axially symmetric tensors, the proton is most shielded, rather than least shielded, when B_0 lies along the ^{13}C–H bond.

Qualitatively, a recognition of this slight "off-resonance" character, even after one adopts a functional definition of being "on-resonance," makes it intuitively more reasonable to expect some non-Lorentzian character to the lineshapes for polycrystalline samples. That is to say, *in an unoriented polycrystalline sample, CW decoupling cannot simultaneously maximize* T_2^C*(ORPI) for the same carbon species in all crystallites.* This effect is fairly minor, however. In fact, the predicted contribution to "on-resonance" linewidths due to their actually being "off-resonance" by 0.6 ppm is typically about 3% (8% maximum) of the measured LW_n(ORPI) values. Note, therefore, that the experimentally observed dispersion in T_{2n}^C(ORPI) between the OR-LPE and the LPE samples is significantly larger than can be accounted for by any such resonance offset.

We digress now to comment on resolution relative to Bloch–Siegert (B–S) shifts (*8, 30*). Since we have implicitly advocated the use of large ν_1^H's in this paper, there is an increased possibility that unwanted line broadening may result from accompanying *inhomogeneous RF fields* which, in turn, produce a distribution of B–S shifts across the sample. We show here that such effects will usually be very small. B–S shifts

originate from the counterrotating portion of the RF field. Expressed in parts per million, the B–S shift on the protons, $\delta^{H}_{B-S}(\nu^{H}_1)$, is

$$\delta^{H}_{B-S}(\nu^{H}_1) = (\nu^{H}_1/2\nu^{H}_0)^2 \qquad [11]$$

while that on the carbons in the presence of CW proton decoupling, $\delta^{C}_{B-S}(\nu^{H}_1)$, is

$$\delta^{C}_{B-S}(\nu^{H}_1) = (\gamma_C/\gamma_H)^2\{(\nu^{H}_1)^2/[(\nu^{H}_0)^2 - (\nu^{C}_0)^2]\}$$
$$= 0.0675(\nu^{H}_1/\nu^{H}_0)^2 = 0.270\delta^{H}_{B-S}(\nu^{H}_1), \qquad [12]$$

where ν^{H}_0 and ν^{C}_0 are, respectively, the Larmor frequencies of the protons and carbons. Clearly the presence of $(\nu^{H}_0)^2$ in the denominator of both expressions tends to make B–S shifts more dominant (in ppm) at lower B_0 since acceptable ν^{H}_1's increase more slowly than B_0 itself. Our concern, however, is not the B–S shifts themselves but B–S *broadening.* Also, we only consider $\delta^{C}_{B-S}(\nu^{H}_1)$ since $\delta^{H}_{B-S}(\nu^{H}_1)$ is a negligible effect for this discussion.

If we suppose ν^{H}_1 is inhomogeneous, covering a range across the sample from $\nu^{H}_1(1-\epsilon)$ to $\nu^{H}_1(1+\epsilon)$, then assuming that $\epsilon \ll 1$, the corresponding range of associated B–S shifts would be about $(4\epsilon)\delta^{C}_{B-S}(\nu^{H}_1)$, centered near $\delta^{C}_{B-S}(\nu^{H}_1)$. As an example, assume $\epsilon = 0.1$. Then $(4\epsilon)\delta^{C}_{B-S}(\nu^{H}_1)$ values for the following pairs of (B_0, ν^{H}_1) apply: 1.4 T, 55 kHz (=0.023 ppm = 0.34 Hz); 2.35 T, 60 kHz (=0.0095 ppm = 0.24 Hz); 4.7 T, 70 kHz (=0.0033 ppm = 0.16 Hz); and 9.4 T, 115 kHz (=0.0022 ppm = 0.22 Hz). Even if $\epsilon = 0.2$, broadening will be limited to about 0.5 Hz, so the Bloch–Siegert broadening is almost negligible. Relative to the issue of RF inhomogeneity it is probably fair to say that the most important advantage of homogeneous RF fields is the increased ability to achieve RF matching across a sample when fixed-amplitude, CW RF fields are used for cross-polarization at higher ν_r (*39*).

Consider, finally, the non-ORPI, linewidth contributions of Fig. 9a. These mainly inhomogeneous contributions were placed into two categories, namely, those accounted for by adamantane linewidths (attributable to B_0 inhomogeneities and Bloch–Siegert effects) and those arising from all the other possible mechanisms including (a) contributions from second-order dipolar effects (more important at lower fields because, expressed in parts per million, these dispersions have a B_0^{-2} dependence), (b) molecular motion (a contribution less than 2 Hz in LPE at ambient temperature), (c) chemical shift dispersion, and (d) anisotropic magnetic susceptibility effects. The interpretation we give to Fig. 9a is that about 0.12 ppm of linewidth in LPE is attributable to reasons (c) and/or (d), where it is recognized that a substance like LPE is a very favorable case relative to mechanism (d) given that aromatic materials often have contributions 5–10 times larger (*4*). The upswing in the LPE data at 1.4 T is most likely to be the consequence of second-order dipolar effects (*13*, *14*).

CONCLUSIONS

Ambient temperature linewidths have been measured for the carbons in the crystalline region of linear polyethylene (LPE) in an unoriented and an oriented sample. The behavior of these carbons should be representative of methylene carbons at natural abundance in other rigid solids. Methine carbons should also show many parallel behaviors. Carryover of these results to methylene linewidths in highly enriched materials should be reasonably good, once allowance is made for the additional line-broadening mechanisms associated with the ^{13}C–^{13}C couplings (*3*).

Measurements have spanned a rather wide range of static field (B_0), RF field strength (ν^{H}_1), MAS frequency (ν_r), and RF-frequency offset ($\Delta\nu_{RF}$). Observed ^{13}C linewidths are made up of both inhomogeneous and homogeneous contributions. The latter contributions tend to become more important at higher B_0, where, in the absence of molecular motion, the T^{C}_2's are dominated by proton chemical shift effects which give rise to line broadening associated with off-resonance proton irradiation (ORPI). Corresponding linewidth contributions are designated LW(ORPI).

By adopting the "effective-field" picture of CW decoupling, we have been able to explain the dependences of LW(ORPI) on B_0, ν^{H}_1, ν_r, and $\Delta\nu_{RF}$. These explanations cover the very different dependences of LW(ORPI) on ν_r when the source of the deviation from proton resonance is a constant, e.g., $\Delta\nu_{RF}$, versus when the source has MAS-modulated, second-rank-tensor properties. Thereby we understand how higher ν_r aids in reducing LW(ORPI) contributions originating from proton chemical shift dispersions and why there is little dependence on ν_r for the LW(ORPI) contributions arising from proton chemical shift anisotropy or from dipolar fields associated with third nuclei.

Estimates of proton spin fluctuation times, τ_s, in the presence of CW decoupling have been made, based on the ν_r dependence of linewidth-versus-$\Delta\nu_{RF}$ plots. In the fitting process for obtaining τ_s and the use of the deduced τ_s for predicting on-resonance values of LW(ORPI), there is also some evidence of a shorter time scale for polarization exchange between protons within a $^{13}CH_2$ group compared to the time scale for exchange between one of these protons and a more distant proton.

This work on the characterization of LW(ORPI) has significance for developing a perspective on the utility of phase modulation schemes like two-pulse phase modulation (TPPM) since TPPM is designed to reduce LW(ORPI) contributions. While the LPE data provide "typical" LW(ORPI) values for a rigid methylene carbon in a rigid hydrocarbon solid, these results will not necessarily be typical for LW(ORPI) when protons experience dipolar fields from third magnetic nuclei or when carbons are embedded in samples containing particles with large magnetic susceptibility. In those cases, LW(ORPI) may be much larger. Yet, this paper gives a framework for predicting these effects.

Since, for LPE, the fraction of the observed linewidth corresponding to LW(ORPI) increases steadily with B_0, TPPM

becomes more inviting at higher B_0. A perspective, however, is that even at $B_0 = 9.4$ T, only about 37–45% of the observed linewidth is attributed to LW(ORPI) for the larger ν_1^H's, where linewidth contributions from MAS-assisted dipolar fluctuations (MADF) are small.

In choosing experimental parameters for good resolution, the LPE data reported herein also indicate that the MADF influence on observed linewidths can be dominant, growing quickly as ν_1^H is reduced. This is a matter of concern, especially because ν_r values much higher than those used herein are now available in commercial probes. Moreover, there is a natural tendency to use a higher ν_r at higher B_0.

One can consider a recipe for a minimum acceptable RF field, $(\nu_1^H)_{min}$, for reasonable CW decoupling. A consideration only of LW(ORPI) would dictate that this field increase approximately as $(B_0)^{1/2}$ in order to preserve constant resolution (in ppm) as one changes B_0. This relationship is predicated on the following assumptions, namely, that the observed linewidth, LW_{ppm} (in ppm) will take the form $k_1 + k_2 B_0 (\nu_1^H)^{-2}$, where k_1 represents an inhomogeneous linewidth contribution, assumed constant in units of parts per million, and k_2 can be obtained from an expression like Eq. [10]. Then, in order to keep LW_{ppm} fixed as a function of B_0, $\nu_1^H = [k_2 B_0/(LW_{ppm} - k_1)]^{1/2}$, i.e., $(\nu_1^H)_{min} \propto (B_0)^{1/2}$. On the other hand, a consideration of MADF effects implies that the main dependence to account for is the ν_r dependence. One tries to choose a $(\nu_1^H)_{min}$ such that one stays above the threshold for the strong broadening illustrated in Fig. 10. From the ν_r dependence of the 9.4 T data shown, we anticipate the following relationship: $(\nu_1^H)_{min} \approx (\nu_1^H)^* + k_m \nu_r$, where $(\nu_1^H)^*$ is the minimum ν_1^H required for avoiding the threshold of MADF contributions in the limit of slow spinning and $2 \leq k_m \leq 3$. If we assume that the maximum ν_r we might wish to use at a given B_0 is proportional to B_0, then $(\nu_1^H)_{min} \approx (\nu_1^H)^* + k_3 B_0$, where k_3 is a constant. The latter expression has a B_0 dependence stronger than that of the condition associated with LW(ORPI). So there is a B_0 (which depends on the maximum ν_r one desires at a particular B_0) above which MADF contributions rather than LW(ORPI) contributions will determine $(\nu_1^H)_{min}$. An important distinction to be dealt with experimentally is whether or not MADF contributions to linewidths are subject to any control via strategies like TPPM; we are doubtful that TPPM will be effective in reducing this contribution. Certainly the existence of strong MADF contributions to linewidth at very high ν_r (≈25 kHz) has been verified (*40*).

The different measurements made on the OR-LPE and LPE samples have pointed to significant orbit-dependent dispersions, in both the homogeneous and the inhomogeneous contributions to linewidth. Moreover, it is demonstrated that in a polycrystalline sample, one cannot simultaneously optimize T_{2n}^C(ORPI) for the same kind of carbon in each crystallite. Lineshape analyses based on assumed Lorentzian or Gaussian lineshapes should be regarded as strictly utilitarian approaches with little underlying justification.

Finally, a brief look at linewidths in crystalline methyl-α-D-glucopyranoside tetraacetate (MGT) indicated that both methylene and methine carbons have behavior which parallels that of LPE in the sense that for modest $\Delta\nu_{RF}$ values, LW_f(ORPI) varies with $(\Delta\nu_{RF})^2$, and for "on-resonance" CW decoupling, (a) MADF effects can be very prominent at lower ν_1^H and/or higher ν_r and (b) one sees an approximately linear dependence of LW_n(ORPI) on $(\nu_1^H)^{-2}$. For methine carbons, however, the latter dependence shows quite varied strengths. It is surmised that this difference in sensitivity is a result of the differing tensor directions for the ^{13}C–H dipolar interaction relative to that of the chemical shift anisotropy of the corresponding proton. A notable difference between the MGT and the LPE results was that the lineshapes in MGT looked more "heterogeneous" (less smooth) than in LPE; this may be a result of the lower proton density in MGT. In contrast to the methylene and methine carbons, the methyl and unprotonated carbons of MGT had greatly reduced dependences of linewidth on $\Delta\nu_{RF}$, ν_1^H, and ν_r, as expected.

This work has elucidated the mechanisms of important T_2^C(ORPI) contributions to linewidth associated with rigid methylene (and methine) carbons in highly protonated solids and has identified that portion of the linewidth, LW(ORPI), which can be dealt with, in principle, with alternate decoupling strategies like TPPM. As mentioned, a very important remaining issue is whether TPPM, or other strategies, can deal with the influence of MAS-assisted dipolar fluctuations. Also, more work needs to be done in other rigid systems that possess both methine and methylene carbons in environments of varied proton density. In LPE, ν_r values up to 8 kHz seemed to cause little change in the intrinsic dipolar fluctuation rates. More information is needed over a wider range of ν_r in order to investigate (a) lineshape behavior in the regime where ν_r begins to lengthen spin lifetimes, and (b) the role that proton distributions have in determining the ν_r at which spin fluctuations begin to slow down.

ACKNOWLEDGMENTS

We thank Dr. R. Tycko of the National Institutes of Health for giving us access to his 9.4 T magnet so that we could conduct our higher field measurements. Also, we thank Professor Ian Ward of the University of Leeds for supplying the sample of drawn LPE. Thanks are due also to K. W. Zilm and A. K. Mehta of Yale University for stimulating discussions and for disclosing unpublished, high-speed-spinning results.

REFERENCES

1. A. E. Bennett, C. M. Rienstra, M. Auger, K. V. Lakshmi, and R. G. Griffin, *J. Chem. Phys.* **103,** 6951 (1995).
2. M. Ernst, S. Bush, A. C. Kolbert, and A. Pines, *J. Chem. Phys.* **105,** 3387 (1996).
3. M. M. Maricq and J. S. Waugh, *J. Chem. Phys.* **70,** 3300 (1979).
4. D. L. VanderHart, W. L. Earl, and A. N. Garroway, *J. Magn. Reson.* **44,** 361 (1981).
5. A. N. Garroway, D. L. VanderHart, and W. L. Earl, *Philos. Trans. R. Soc. London A* **299,** 609 (1981).

6. B. H. Meier and W. L. Earl, *J. Am. Chem. Soc.* **107,** 5553 (1985).
7. D. Suwelack, W. P. Rothwell, and J. S. Waugh, *J. Chem. Phys.* **73,** 2559 (1980).
8. M. Mehring, "Principles of High Resolution NMR in Solids," Springer-Verlag, Berlin (1976).
9. K. Takegoshi and C. A. McDowell, *J. Magn. Reson.* **66,** 14 (1986).
10. T. K. Pratum, *J. Magn. Reson.* **88,** 384 (1990).
11. T. K. Pratum, *Chem. Phys. Lett.* **172,** 291 (1990).
12. D. P. Raleigh, C. P. Grey, N. Soffe, and C. M. Dobson, *J. Magn. Reson.* **97,** 162 (1992).
13. D. L. VanderHart, *J. Chem. Phys.* **84,** 1196 (1986).
14. M. P. Augustine, K. W. Zilm, and D. B. Zax, *J. Chem. Phys.* **98,** 9432 (1993).
15. F. Horii, A. Hirai, and R. Kitamaru, *Polym. Bull.* **8,** 163 (1982).
16. H. Saito, R. Tabeta, A. Shoji, T. Ozaki, and I. Ando, *Macromolecules* **16,** 1050 (1983).
17. D. L. VanderHart, *J. Magn. Reson.* **44,** 117 (1981).
18. G. E. Pake, *J. Chem. Phys.* **16,** 327 (1948).
19. A. Abragam, "The Principles of Nuclear Magnetism," Chap. 2, Oxford Univ. Press, London (1962).
20. A. Samoson, E. Lippmaa, and A. Pines, *Mol. Phys.* **65,** 1013 (1988).
21. A. Llor and J. Virlet, *Chem. Phys. Lett.* **152,** 248 (1988).
22. K. T. Mueller, B. Q. Sun, G. C. Chingas, J. W. Zwanziger, T. Terao, and A. Pines, *J. Magn. Reson.* **86,** 470 (1990).
23. G. Sinning, M. Mehring, and A. Pines, *Chem. Phys. Lett.* **43,** 382 (1976).
24. A. Pines, W.-K. Rhim, and J. S. Waugh, *J. Magn. Reson.* **6,** 457 (1972).
25. D. L. VanderHart and A. N. Garroway, *J. Chem. Phys.* **71,** 2773 (1979).
26. Certain commercial companies are named in order to specify adequately the experimental procedure. This in no way implies endorsement or recommendation by the authors or their agencies.
27. D. A. Torchia, *J. Magn. Reson.* **30,** 613 (1978).
28. R. Kitamaru, F. Horii, and K. Murayama, *Macromolecules* **19,** 636 (1986).
29. T. Nakai and C. A. McDowell, *Chem. Phys. Lett.* **227,** 639 (1994).
30. F. Bloch and A. Siegert, *Phys. Rev.* **57,** 552 (1940).
31. M. G. Munowitz and R. G. Griffin, *J. Chem. Phys.* **78,** 613 (1983).
32. D. A. McArthur, E. L. Hahn, and R. Walstedt, *Phys. Rev.* **188,** 609 (1969).
33. D. E. Demco, J. Tegenfeldt, and J. S. Waugh, *Phys. Rev. B* **11,** 4133 (1975).
34. P. Tekely, P. Palmas, and D. Canet, *J. Magn. Reson. A* **107,** 129 (1994).
35. J. R. Havens and D. L. VanderHart, *J. Magn. Reson.* **61,** 389 (1985).
36. X. Wu, S. Zhang, and X. Wu, *Phys. Rev. B* **37,** 9827 (1988).
37. E. O. Stejskal, J. Schaefer, and J. S. Waugh, *J. Magn. Reson.* **28,** 105 (1977).
38. E. Hagaman, *J. Magn. Reson.* **104,** 125 (1993).
39. X. Wu and K. Zilm, *J. Magn. Reson. A* **104,** 154 (1993).
40. A. K. Mehta, B. A. Tounge, S. T. Burns, and K. W. Zilm, 38th Experimental NMR Conference, Poster 262, Orlando FL, 1997.